AFRL-RV-PS-
TR-2014-0181

DEVELOPMENT AND APPLICATION OF NUMIT FOR REALISTIC MODELING OF DEEP-DIELECTRIC SPACECRAFT CHARGING IN THE SPACE ENVIRONMENT

Brian P. Beecken

Bethel University
3900 Bethel Drive
St. Paul, MN 55112-6999

21 April 2014

Final Report

AIR FORCE RESEARCH LABORATORY
Space Vehicles Directorate
3550 Aberdeen Ave SE
AIR FORCE MATERIEL COMMAND
KIRTLAND AIR FORCE BASE, NM 87117-5776

DTIC COPY

NOTICE AND SIGNATURE PAGE

Using Government drawings, specifications, or other data included in this document for any purpose other than Government procurement does not in any way obligate the U.S. Government. The fact that the Government formulated or supplied the drawings, specifications, or other data does not license the holder or any other person or corporation; or convey any rights or permission to manufacture, use, or sell any patented invention that may relate to them.

This report was cleared for public release by the 377 ABW Public Affairs Office and is available to the general public, including foreign nationals. Copies may be obtained from the Defense Technical Information Center (DTIC) (http://www.dtic.mil).

AFRL-RV-PS-TR-2014-0181 HAS BEEN REVIEWED AND IS APPROVED FOR PUBLICATION IN ACCORDANCE WITH ASSIGNED DISTRIBUTION STATEMENT.

//SIGNED//	//SIGNED//
Dr. David Cooke	Glenn M. Vaughan, Colonel, USAF
Project Manager, AFRL/RVBX	Chief, Battlespace Environment Division

This report is published in the interest of scientific and technical information exchange, and its publication does not constitute the Government's approval or disapproval of its ideas or findings.

REPORT DOCUMENTATION PAGE

Form Approved
OMB No. 0704-0188

1. REPORT DATE *(DD-MM-YYYY)*	**2. REPORT TYPE**	**3. DATES COVERED** *(From - To)*
21-04-2014	Final Report	28 Apr 2011 – 21 Apr 2014

4. TITLE AND SUBTITLE
Development and Application of NUMIT for Realistic Modeling of Deep-Dielectric Spacecraft Charging in the Space Environment

5a. CONTRACT NUMBER
FA9453-11-C-0250

5b. GRANT NUMBER

5c. PROGRAM ELEMENT NUMBER
63401F

6. AUTHOR(S)
Brian P. Beecken

5d. PROJECT NUMBER
5021

5e. TASK NUMBER
PPM00011420

5f. WORK UNIT NUMBER
EF004167

7. PERFORMING ORGANIZATION NAME(S) AND ADDRESS(ES)
Bethel University
3900 Bethel Drive
St. Paul, MN 55112-6999

8. PERFORMING ORGANIZATION REPORT NUMBER

9. SPONSORING / MONITORING AGENCY NAME(S) AND ADDRESS(ES)
Air Force Research Laboratory
Space Vehicles Directorate
3550 Aberdeen Avenue, SE
Kirtland AFB, NM 87117-5776

10. SPONSOR/MONITOR'S ACRONYM(S)
AFRL/RVBX

11. SPONSOR/MONITOR'S REPORT NUMBER(S)
AFRL-RV-PS-TR-2014-0181

12. DISTRIBUTION / AVAILABILITY STATEMENT
Approved for Public Release; distribution is unlimited. (377ABW-2014-0976 dtd 04 Dec 2014)

13. SUPPLEMENTARY NOTES

14. ABSTRACT
NUMIT has been refined, developed, and greatly enhanced so that it can be used to model and predict the deep charging of dielectrics on spacecraft. The new tool, called AF-NUMIT2, can now model isotropically incident electron fluxes from realistic energy spectra that change with time. The model has been extended to incident electron fluxes an order of magnitude lower than before (>= 10 keV), and aspects of the model have been checked against Monte Carlo simulations. Electron energy flux spectra, as measured by CRRES, have been used in dozens of simulations of Kapton charging over multiple days. Kapton has been modeled with both dark conductivities and radiation induced conductivities extending over two orders-of-magnitude. The result is a surprisingly consistent relationship between maximum internal electric field strengths and conductivity, regardless of the particular incident electron spectra.

15. SUBJECT TERMS
NUMIT, deep-dielectric charging, modeling charging

16. SECURITY CLASSIFICATION OF:			**17. LIMITATION OF ABSTRACT**	**18. NUMBER OF PAGES**	**19a. NAME OF RESPONSIBLE PERSON**
a. REPORT	**b. ABSTRACT**	**c. THIS PAGE**			Dr. David Cooke
Unclassified	Unclassified	Unclassified	Unlimited	58	**19b. TELEPHONE NUMBER** *(include area code)*

Standard Form 298 (Rev. 8-98)
Prescribed by ANSI Std. 239.18

This page is intentionally left blank.

TABLE OF CONTENTS

LIST OF FIGURES

This page is intentionally left blank.

1.0 SUMMARY

A one-dimensional software tool designed for laboratory modeling (NUMIT) has been refined, developed, and greatly enhanced so that it can be used to model and hopefully predict the deep-dielectric charging of dielectrics on spacecraft. The new tool, called AF-NUMIT2, can now model isotropically incident electron fluxes from realistic energy spectra that change with time. The model has been extended to incident electron fluxes an order of magnitude lower than before (from >100 keV to > 10 keV), and aspects of the model have been checked against Monte Carlo simulations. In order to verify the utility of AF-NUMIT2, dozens of simulated runs have been made using realistic, isotropic electrons incident on Kapton, representing a wide range of actual energy spectrum fluxes measured by CRRES. Kapton has been modeled with both dark conductivities and radiation induced conductivities extending over two orders-of-magnitude. The result has been a surprisingly consistent relationship between maximum internal electric field strengths and conductivity.

2.0 INTRODUCTION

The original NUMIT, short for *num*erical *it*eration, was designed and described by A. R. Frederickson. [1] [2] It was a one-dimensional model intended primarily to aid in the interpretation of laboratory testing during which mono-energetic electron beams had normal incidence on various dielectric slabs. The basic concepts of NUMIT have been utilized in the present work and must be understood before the development of AF-NUMIT2 can be explained. NUMIT necessarily combines three different algorithms or models: energy deposition, electron deposition, and charge transport. Summarized here are the primary algorithms used when the author worked with Frederickson in 2000:

1. **EDEPOS** An algorithm is required to determine the deposition of energy as a function of depth by the incident, high-energy electrons. NUMIT accomplishes this by utilizing the well-known EDEPOS algorithm, [3] which in fewer than fifty lines of code compiles the results of numerous experiments and Monte Carlo simulations for various materials and incident electron energies.
2. **FredBell** An algorithm is required to determine where the incident electrons stop in the dielectric as a function of depth. We use an algorithm by Frederickson, Bell, and Beidl [4] that draws heavily on EDEPOS and incorporates Monte Carlo simulations. For convenience, we name this algorithm “FredBell.”
3. **Transport Model** A transport model is required to determine how the charge moves about within the dielectric. NUMIT determines the conductivity in the dielectric that results from the energy deposition by utilizing the well-known Fowler Model [5] for radiation induced conductivity (RIC). Then, the current can be predicted once electrostatics is used to calculate the electric field resulting from the charge deposition.

Recent work has shown that internal electric fields are the best predictor of deep-dielectric pulsing. [6] [7] Therefore, it is the calculation of the electric field internal to the dielectric, and the prediction of how it might change in time, that makes NUMIT a potentially useful approach for assisting the spacecraft designer.

Frederickson's original algorithm has been greatly expanded and enhanced during the course of the present contract in order to enable NUMIT to model what might be happening to dielectrics in space. The development of a limited, laboratory modeling code into a more sophisticated code AF-NUMIT2 that is useful for predicting the impact of the space environment on Air Force systems is a multifaceted task. The goals, as delineated in the SOW, are listed here with only the order changed to reflect the sequence in which they are addressed in the present report:

1. (Sec 3.2) Establishment of a definitive, controlled source code for AF-NUMIT2
2. (Sec 3.3) Method for accounting for electrons incident at different angles
3. (Sec 3.4) Provision for arbitrary electron energy spectrums
4. (Sec 3.5) Provisions for time-sequenced incident electron flux environments
5. (Sec 3.6) Extension of model for incident electrons to lower energy range
6. (Sec 3.7) Verification of the energy deposition model in NUMIT
7. (Sec 3.8) Development of time-delayed and temperature-dependent radiation induced conductivity algorithms

A detailed discussion of each of these goals will be in the next section.

3.0 METHODS, ASSUMPTIONS, AND PROCEDURES

3.1 The Original NUMIT Algorithms

The plan for the work reported here was to lean heavily on the original methods and assumptions utilized by Frederickson in his NUMIT simulation in order to devise a method of predicting the electric fields that develop within spacecraft dielectrics subjected to the space environment. Frederickson utilized three algorithms for his one-dimensional laboratory model, each of which have been modified as part of the development of AF-NUMIT2. Accordingly, each will be described briefly in this section.

3.1.1 Energy Deposition Profile (EDEPOS). EDEPOS (short for *e*nergy *depos*ition) was created in 1974 by Tabata and Ito [3] and has become an important and widely used algorithm for determining the profile of energy deposition by normally incident electrons. EDEPOS uses the results of more than twenty experimental studies and more than a half-dozen Monte Carlo method calculations. At the time, the leading algorithm had been produced by Kobetich and Katz [8], but Tabata and Ito demonstrated that their version was valid over a wider range of incident energies with greater accuracy.

In addition to the energy of the incident mono-energetic electrons, EDEPOS requires only the input of the insulator's atomic number, atomic weight, and density. Effective atomic numbers can be used so that the range of applicability is from about 5.3 to 82. The incident electron energy

range is 0.1–20 MeV. The algorithm was published as only forty-five lines of FORTRAN code. [3] Its ready availability, rapid computation time, wide applicability, and ease of use has made EDEPOS a tool of choice for many modelers. The output of EDEPOS, when multiplied by the incident electron beam current J_{inc}, is the energy deposition profiles, the dose rate $\dot{D}(x)$, required to determine RIC in NUMIT.

3.1.2 Incident Electron Deposition Profile (FredBell). In order to model the movement of charge within the dielectric, one must know where the high-energy incident electrons stop. In 1995, Frederickson, Bell, and Beidl [4] produced an algorithm that superseded all earlier guesses at where the charge was being deposited. Frederickson et al. took Tabata's EDEPOS and modified it, using equations that "crudely" simulated physical processes. These equations were then assembled into an algorithm with six fitting parameters. By comparison with Monte Carlo simulations, Frederickson was able to determine analytical functions for five of the six parameters. He left the sixth (called "*B*") to be determined from a six-column table.

Because it draws on the energy deposition algorithm by Tabata, the FredBell algorithm requires use of EDEPOS—it cannot be used as a stand-alone algorithm. The required inputs are the same as for EDEPOS, and the output is the fraction of incident electron flux as a function of depth. When multiplied by the incident electron beam current J_{inc}, FredBell provides the initial electron current profile $J_0(x)$ that is required in NUMIT.

3.1.3 Charge Transport Algorithm. Once the energy and electron deposition are determined as a function of depth in the dielectric, NUMIT creates a transport algorithm based on electrostatics and Fowler's conductivity model. [5] Although NUMIT can be modified for different configurations, the simplest setup is illustrated in Figure 1. A dielectric slab is sandwiched between two electrodes that can be held at the same electric potential or at a fixed potential difference.

In Figure 1, we take the left side of the dielectric to be $x = 0$ and measure the depth from that point. The incident high-energy electrons are assumed to come from the left and penetrate into the dielectric. For the purposes of modeling, the left electrode can be taken to be immeasurably thin, such as conductive paint. Initially, in the absence of an accumulation of charge, the incident electrons create a position-dependent current density $J_0(x)$.

The initial current density is virtually always a monotonically decreasing function of depth x because the electrons are slowed and absorbed by the dielectric, and significantly fewer electrons reach the far side than enter the dielectric. As the electrons are absorbed, they give up their energy to the dielectric. The rate of this energy deposition is called the dose rate $\dot{D}(x)$ and is given in rad/sec. Unlike $J_{0,}$ the dose rate is not a monotonically decreasing function of x, but typically peaks before exhibiting a tail. In NUMIT, $\dot{D}(x)$ and $J_0(x)$ are approximated by the EDEPOS and FredBell algorithms discussed above.

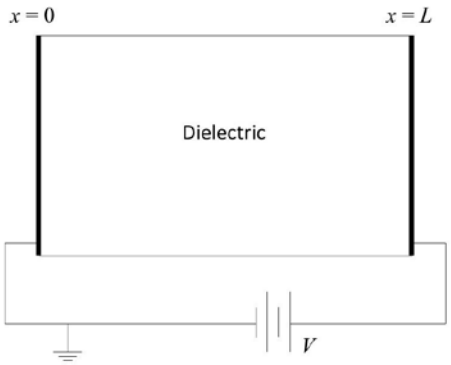

Figure 1. Schematic Diagram of Situation Modeled by NUMIT

As shown in Figure 1, the left electrode at $x = 0$ is grounded, while the right electrode at $x = L$ is held at a constant potential *V*, which very often is set to zero. The dielectric is assumed to have a constant permittivity ϵ. Its thickness *L* is assumed to be small compared to its other dimensions so that the problem can be treated in one dimension. We wish to find the charge density ρ, the electric field *E*, and the current density *J* as functions of position *x* and time *t*.

There are three major equations required to relate ρ, *E*, and *J*. The first two are the continuity equation and the differential form of Gauss's Law. In one-dimension, these are

$$\frac{\partial J(x,t)}{\partial x} = \frac{\partial \rho(x,t)}{\partial t} \tag{1}$$

and

$$\frac{\partial E(x,t)}{\partial x} = \frac{\rho(x,t)}{\epsilon} \tag{2}$$

The third equation required represents the transport of charge. Utilizing the Fowler Model for radiation induced conductivity, we see that for the same electric field, the current will be higher when the dose rate is greater:

$$J(x,t) = J_0(x) + \left[g_0 + k\dot{D}(x)\right]E(x,t) \tag{3}$$

Here g_0 is the dark conductivity, *k* is the coefficient of radiation-induced conductivity (RIC), and $\dot{D}(x)$ is the dose rate. The dark conductivity is the conductivity of the insulator when it is not radiated. Because it is an insulator, the dark conductivity is extremely low and difficult to

determine accurately for many important materials—particularly in space applications. [9] [10] [11] [12]

Equations (1)–(3) can be used to describe the transport of charge in the dielectric by taking successive time steps. The initial current $J_0(x)$ is due to the incident high-energy electrons and is given by the FredBell algorithm. Then the Continuity Equation (1) enables us to find the charge deposited $\rho(x, \Delta t)$ a moment Δt in time later. Once we know $\rho(x, \Delta t)$, Gauss's Law (2) enables us to find $E(x, \Delta t)$. Combining our knowledge of $E(x, \Delta t)$ with the dose rate $\dot{D}(x)$ given by the EDEPOS algorithm, Equation (3) enables us to determine the movement of the deposited charge. Of course, electrons continue to be incident on the material so $J_0(x)$ must be added to find the new total current $J(x, \Delta t)$ within the dielectric. This cyclical time stepping process can continue as long as desired or until equilibrium is achieved.

The numerical algorithm requires careful choice of the sizes of the spatial increment Δx across the dielectric and the time step size Δt. The choice of Δx determines the resolution of all the calculated values, but too small a value will make the simulation take longer than necessary. Each Δx can be thought of as a *bin* which holds the charge in that region of the dielectric. The charge is considered to reside in the center of each bin, called a *node*. For normally incident electrons, the situation for which NUMIT was originally designed, 30–200 nodes usually provide adequate resolution. However, when isotropically incident electrons are included, the number of nodes should normally be increased because deposition will trend shallower. In AF-NUMIT2, even when considering electrons incident at angles other than perpendicular to the surface, the spatial nodes continue to represent the perpendicular depth from the surface.

Similarly, the time step Δt must be chosen very carefully. If it is too small, the program runs for an excessively long time, diminishing its usefulness. If it is too large, the net charge begins to fluctuate wildly. The fluctuations occur because if a time step is too long, then the algorithm will calculate more charge having been removed from the node than the corresponding bin actually holds.

Additional details on NUMIT, including updated calculations of surface charging on the electrodes, can be found elsewhere.[1] [13]

3.2 Establishment of a Definitive, Controlled Source Code for AF-NUMIT2

The original NUMIT was written by Frederickson in FORTRAN. Input and output was very tedious and required the use of another software application for decent plots of the results. When the author worked with Frederickson in 2000, and inserted the FredBell algorithm for the first

[1] See also Brian P. Beecken, "Development of the NUMIT Simulation for Modeling Deep-dielectric Charging in the Space Environment," a report to AFRL/RVBX, August 13, 2009, particularly Appendix A.

time, the FORTRAN code had about half its lines and subroutines commented out. In 2007, the group at JPL responsible for continuing Frederickson's work after his death wrote "NUMIT has not been configuration controlled." [14]

At the time of his inclusion of the FredBell algorithm, the author discovered that the way it handled delta ray current[2] could not be utilized without double precision in FORTRAN. For expediency, in consultation with Frederickson, it was decided to leave out delta rays because they were a relatively small effect. FredBell was also limited in usefulness by the requirement of looking up a parameter called "B" in a published table. Each change of material and/or energy required finding the appropriate value for B in the table and inserting it manually in the code. These limitations have recently been independently documented and corrected at JPL. [15]

AF-NUMIT2 is written in MATLAB™ which allows for easy input of relevant parameters and the rapid output of publication quality graphs, and it is inherently comparable to double precision in FORTRAN. The subroutines EDEPOS and FredBell have been adjusted and combined into one MATLAB function named BeeckenTabFred. The code accounts for delta ray current and has been revised for efficiency so that it runs significantly faster. Speed improvements are important because AF-NUMIT2 requires many loops through this function as it simulates the space environment with isotropically incident electrons. A short function called "getparameterB" was written to interpolate the Frederickson table for "B", and it allows the program to run without additional user inputs.

Figure 2 is a flow chart for AF-NUMIT2. The blue Time Loop portion is essentially the original NUMIT as described above, written in MATLAB with the aforementioned enhancements. The yellow Spectrum Loop block represents the bulk of the additions that had to be made to the code in order to predict charging in realistic space environments. The green Inputs block describes the far more complicated inputs that are required for the program to model the space environment, and the red Plotting block illustrates the new standard outputs.

[2] Delta ray current is a name for electrons that are knocked loose in the material by the high-energy incident electrons. On average they move deeper within the material.

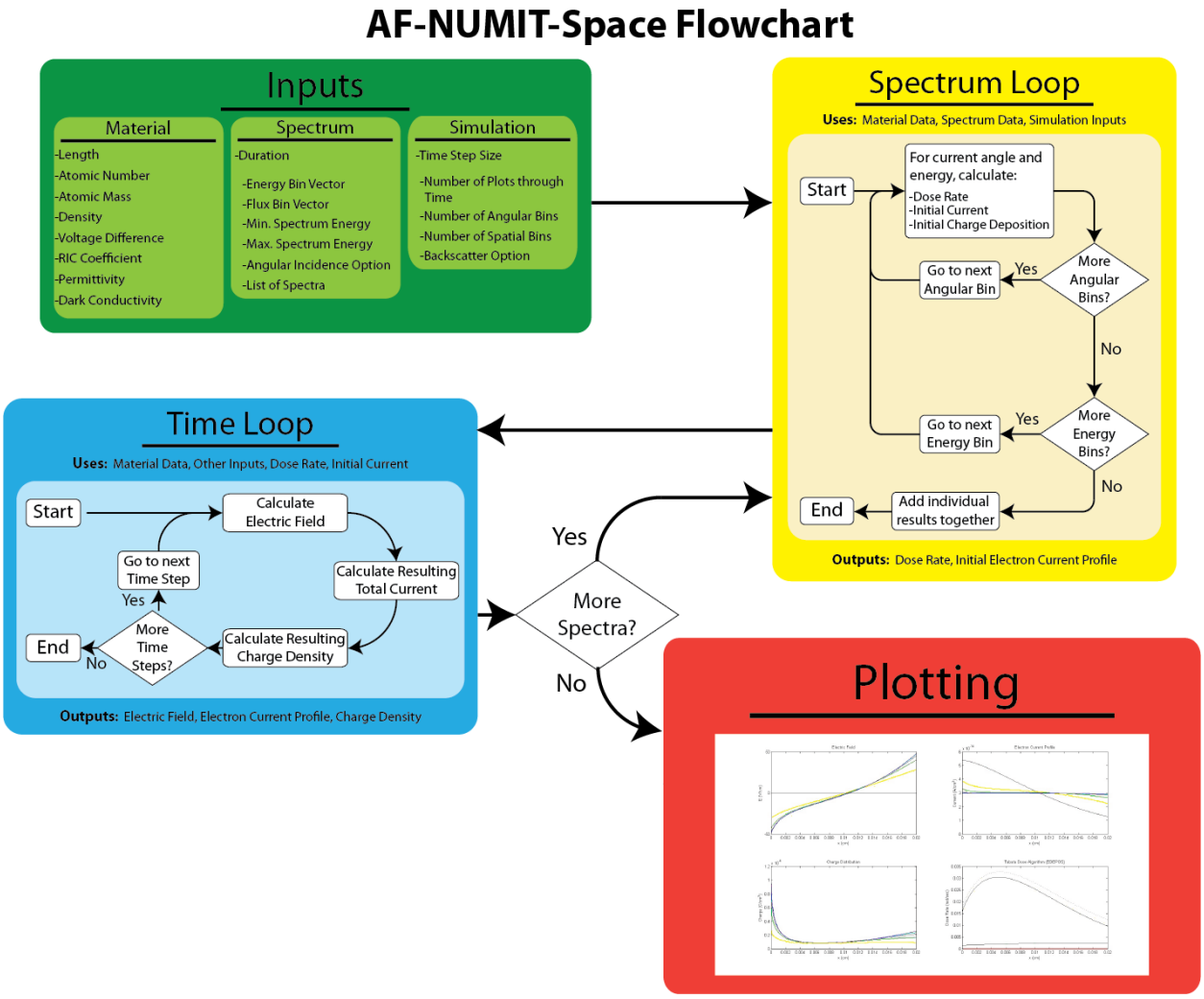

Figure 2. Flow Chart for AF-NUMIT2

AF-NUMIT2 has been produced in two versions. The first is written as a standard Matlab™ program with extensive commenting. It is purposely designed to be easily modified and improved by users who have some familiarity with Matlab. Instructions on its use, the first 100 lines of code necessary for inputs, and a list explaining the variables used within the code (to aid in modification), have been provided in Appendices A, B, and C. Calculation of effective atomic number and weight for composite materials is explained in Appendix D. The second version of AF-NUMIT2 has a Graphical User Interface. It contains the same algorithms, but should be an easier version of AF-NUMIT2 to use initially. Unfortunately, it runs much slower and currently is somewhat flaky. Therefore, as of this writing, that version is not being submitted, nor was it included in the SOW. There has been no provision to copyright AF-NUMIT2 or otherwise give it configuration control.

3.3 Method for Accounting for Electrons Incident at Different Angles

A primary limitation in the conversion of NUMIT from a laboratory tool to a model useful for spacecraft design is not that NUMIT is a one-dimensional model of charge transport, but rather it is NUMIT's inherent use of an electron beam that strikes the dielectric surface at only normal incidence. Many dielectrics of interest on spacecraft are essentially flat, so the one-dimensional model of charge transport within the dielectric is an appropriate approximation. The issue then is what is the appropriate way to handle an isotropic flux of electrons striking the surface?

3.3.1 Determination of Electron Flux as a Function of Incident Angle. The determination of the correct electron flux to use is non-trivial. The space environment nominally has an isotropic electron flux. For a particular angle from the normal θ, we need to find the appropriate fraction $J_{inc}(\theta)$ of the total flux that will strike the dielectric surface and then penetrate. What is the appropriate incident flux as a function of angle?

Getting the correct angle dependent incident electron flux is absolutely crucial to a realistic prediction of spacecraft charging. Accordingly, much effort has been expended, and two approaches have been considered and discarded. At first, it might seem reasonable to assume that the calculation is merely the usual determination of the number of electrons that strike the top surface of a disk in an isotropic flux. Such a calculation is well-known, but not relevant because we are interested in penetrating flux. Secondly, it might seem that we need to know the amount of charge that penetrates and then passes through the imaginary line drawn normal to the surface along which the one-dimensional charge transport algorithm will proceed. Significant work was done on this possible approach to calculate the appropriate $J_{inc}(\theta)$ for such a situation, and it was reported in two published proceedings papers. [13] [16] Unfortunately, this approach also appears now to be incorrect. The simplest explanation for the error is conceptual. Because an imaginary line normal to the surface has no thickness, a calculation of particle flux passing through it can have no physical significance.

The correct approach is to consider the flat dielectric as being large enough that there are no edge effects. With the incident electron flux being uniformly isotropic, the deposition of charge within the material will be a function of depth uniformly throughout the material. In other words, for a given depth, the layer of deposited charge at that depth is uniform.

Going back to the calculation of the number of electrons incident on the surface of a disk to determine how the incident flux depends on angle, however, is incorrect because it treats the electrons as electromagnetic radiation. A radiation calculation thinks in terms of the effective area of the detector surface as a function of angle—one that shrinks as the angle of incidence, measured from the normal, increases. However, the implicit, but usually unstated, assumption is non-penetration. For penetrating electrons, see Figure 3, there would be no

such thing as effective area as all electrons that are incident go into the material regardless of angle (neglecting backscatter effects). This change in treatment required much thought, many trial calculations, and was considered at great length with members of AFRL/RVBX.[3] The result is stunningly simple: for isotropic flux, the incident flux is the same at all angles. For AF-NUMIT2, the calculation of the electron current per unit area J_{inc} is done simply by taking the incident flux J_{incident} given in units of (1 / cm^2 sr sec) at a specific energy and multiplying by the steradians in one hemisphere so as to include all electrons incident on the material:

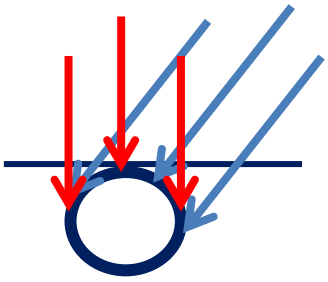

Figure 3. Illustration of Penetrating Model

$$J_{\text{inc}} = 2\pi J_{\text{incident}}.$$

If this treatment is correct, the incident flux does not depend on angle.[4] However, for the purposes of AF-NUMIT2, electrons striking at different angles must be treated differently because they will have different penetration depths. Therefore, the model must keep track of incident angles and this is done by dividing the flux into angular bins of size 2ψ (measured in degrees) at each angle θ. The result is

$$J_{\text{inc}}(\theta) = \frac{2\psi}{90^{\text{o}}} J_{\text{inc}}$$

Note that the fraction must use angles not steradians because the horizontal direction from which the electrons come does not matter. We only want the fraction of all incident electrons at a certain angle θ to the normal.

3.3.2 Determination of Energy and Electron Deposition Profiles as Functions of Angle. We make the assumption that most dielectrics of interest are going to be isotropically homogeneous (certainly not crystalline). Of course many dielectrics will be polymers, but we have to start somewhere. We hope that the polymer chains are not consistently oriented in the same direction so that incident electrons will not penetrate significantly more in one direction than another. If homogeneity is a reasonable approximation, then as the incident high-energy electrons travel through the dielectric in the direction of their straight line trajectory (at a particular angle of incidence) the depth of penetration and the rate of energy deposition should be relatively

[3] We are grateful to William (Bob) Johnston for significant and helpful conversations during August of 2011 and to David Cooke, Dale Ferguson, and Adrian Wheelock for a long discussion and eventual consensus on this approach at a meeting on 25 July 2012.

[4] In the AF-NUMIT2 code, J_{incident} is for specific energy channels, just as it is here. However, in the code, instead of J_{inc} in terms of (1/cm^2) we actually use J_{incid} which is (A/cm^2).

independent of the angle. We are talking strictly about the situation *after* the electrons have entered the material. As we have already shown, the number of electrons striking the material is believed to be angle independent. The number of electrons that are potentially backscattered, however, is obviously angle-dependent and is considered in the next subsection.

Now we can use the EDEPOS and FredBell algorithms (whether separately or in their combined form BeeckenTabFred) to approximate energy and charge depositions for any particular angle of incidence θ. On average, electrons will travel the same distance within the material, however that distance must be scaled back to a perpendicular depth—a simple trigonometric correction. If we call *x* the perpendicular distance into the material, what NUMIT treats as depth, then the distances along the path at an angle of incidence θ given by BeeckenTabFred can be called x_θ. The appropriate conversion becomes:

$$x_\theta \cos\theta = x$$

The BeeckenTabFred algorithm will return to AF-NUMIT2, at various perpendicular depths measured in *x*, the values for the energy deposited per electron (EDEPOS) and the fraction of electrons (Jofrac) that continue on in the chosen direction determined by the incident angle. Both values must be multiplied by a factor representing the current density of electrons that entered the material at a particular angle θ from the normal. This approach is clearly an approximation. However, if isotropic incidence is going to be included in AF-NUMIT2, in the absence of a better approach we must do something. The validity of this approach has been examined using Monte Carlo simulations; it will be discussed in Subsection 3.7.4.

3.3.3 The Issue of Backscatter. When electrons are incident on a material, it is known that some of the electrons penetrate while others are reflected or backscattered. Very little, if any, data is known to exist for backscattering from dielectric materials—particularly as a function of angle. The problem is complicated by secondary electron yields, auger electrons, and differing material structures.[5] Nevertheless, there is a real effect. Certainly it will be angle dependent, and something must be done to at least make an approximation for the sake of AF-NUMIT2 charging predictions. The approach we took is explained here.

Because of backscatter, it is necessary to correct the incident flux by a transmission factor 1-*B*, where *B* is the fraction of electrons that backscatter. When Frederickson developed the FredBell algorithm for electron current and deposition, [4] working at that time strictly with normal incidence, his *B* term depended on electron energy and the material's atomic number. Later,

[5] During a meeting on 15 August 2011 at AFRL/RVBX, several relevant comments were made such as: "Backscatter yields on dielectrics might not exist, even for normal incidence." "The Nascap model is not helpful." "How can such basic data not be available?"

Frederickson developed another equation that included dependence on incident angle θ, in addition to the incident electron energy T_o and the atomic number Z:

$$B = (0.14 - 0.039T_o)(0.1Z^{0.9}) + \frac{0.276\theta^2}{Z^{0.12}}$$

This equation for backscatter was reported in Appendix A.1.2 in a paper by Davis. [17] It would seem obvious that the fraction of electrons backscattering will change as the angle of incidence changes, and this equation seems to provide a realistic estimate of that dependence on angle.

The transmission factor should be unity when the backscatter fraction *B* is zero. Unfortunately, for close to normal incidence, this equation becomes negative for higher electron energies. In such cases, using it will result in a transmission factor greater than unity. Having more electrons in the simulation than are actually incident on the dielectric would seem to reduce realism. It is the first term in *B* that can go negative. Therefore, we have modified the equation in AF-NUMIT2 by normalizing the entire expression, but only when the first term goes negative. Typical results are presented in Figure 4.

Close examination of Figure 4 shows that at the 5 MeV incident electron energy more backscatter occurs at lower atomic numbers, whereas at 1 MeV less backscatter occurs at lower atomic numbers. This difference is inherent in the equation for *B* and is *not* caused by our normalization at the higher energy. The crossover occurs at about 3 MeV. We do not know if this is a realistic representation of the actual situation.

3.3.4 Putting it all together: The Incident Angle Loop. We have shown that there are at least three steps necessary to handle isotropic incidence: determining the electron flux as a function of

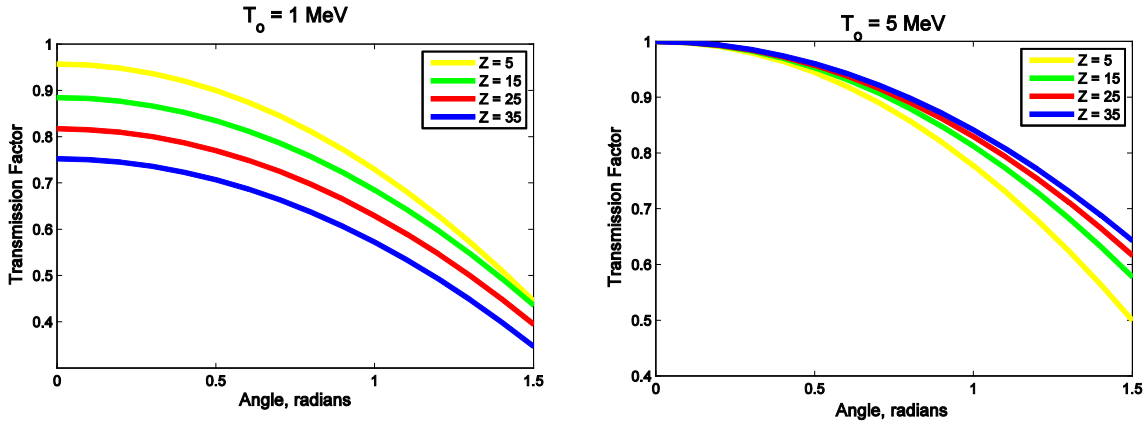

Figure 4: Sample Plots of Transmission after Backscatter

angle, calculating the current and energy deposition profiles in the dielectric that result from

electrons at that angle, and allowing for a dependence on incident angle of the backscattered electrons. But how is this accomplished in the code?

The code must consider each angle of incidence separately. The angles of incidence θ are divided into *angular bins*, the size of these correspond to the resolution chosen by the user. A typical number of bins might be 18 between normal incidence and 90º, correlating to 5º for each angular bin (called 2Ψ) with θ centered within the bin. As illustrated in the Flow Chart of Figure 2, a loop is instituted for each angular bin. Each time through this loop the function BeeckenTabFred calculates the energy and electron deposition profiles. After these profiles are determined for each angle θ, the main AF-NUMIT2 program adds the charge deposited in each spatial bin and separately adds the energy deposited in each spatial bin. As in the original NUMIT, the spatial bins are simply defined as distance (or depth) increments of Δx from the surface as measured perpendicularly.

AF-NUMIT2 will by default use the backscatter function. Although its validity and accuracy is uncertain, it is important to account for backscatter when considering isotropic scattering. Otherwise, due to the large number of electrons incident at very shallow angles (large θ), surface charging will unrealistically dominate a model designed to predict deep-dielectric charging.

3.3.5 Electron Beams. AF-NUMIT2 still does electron beams, either mono-energetic or multi-energetic. The number of angular bins must simply be set to one. Other input differences required for beams are described in Section 3.4.

3.4 Provision for Arbitrary Electron Energy Spectrums

The original NUMIT, being designed for a mono-energetic electron beam, did not have provision for the wide spectrum of energies that electrons incident in a space environment carry. Two aspects of AF-NUMIT2 had to be developed to address this situation: simultaneous modeling of multiple electron energies and the input of those energies.

3.4.1 Modeling multiple electron energies. AF-NUMIT2 has an energy loop as shown in the yellow Spectrum Loop block of Figure 2. For each designated incident electron energy, the code utilizes the function BeeckenTabFred to calculate a depth profile of the energy deposited per electron and the fraction of electrons that continue on for all incident angles. These values are then multiplied by the electron flux at that energy to provide as a function of depth the energy dose rate (Dose_energies), the initial electron current (Jo_energies), and the charge deposition

(rho_energies) at that particular energy. [6] The loop is repeated for each energy in the spectrum. After calculating for all energies, the results are summed to provide dose rate (Dose), initial current (Jo), and deposited charge (rho) as a function of depth in the dielectric. These results are then provided to the transport code shown in the blue Time Loop block of Figure 2.

3.4.2 Input of electron energy spectrums. In order to input the energy spectrum, the user creates a comma-delimited file (.csv). The file contains a minimum of two rows. The first cell must have always have a zero entered in it as a place holder in the comma-delimited file. After that, each cell in the first row will list the energy of a channel in MeV. The first cell of the second row will give the number of seconds that the energy spectrum being modeled is incident. The rest of the cells in the second row will give the electron flux in 1/(cm^2 sr sec MeV) of the energy channel listed above it. An illustrative example, with energy channels 0.5, 1.0, 2.0, 5.0, 10, 20 MeV is provided in Table 1. In this table, there are two rows with differing electron flux values that run for 100 and 150 seconds. More discussion on the input of incident electron flux environments is reserved for Section 3.5.

Once AF-NUMIT2 reads the file, it calculates the size of each energy channel in MeV. With the exception of the first and last energy channels, the energy width is calculated from half the distance in MeV to the channel on either side.[7] For the energy channels on either end of the spectrum, the half distance to the next channel is doubled. In Table 1 this width would be 0.5 MeV for the first channel and 10 MeV for the last channel. The second channel has a width of 0.75 MeV, the third has 2.0 MeV and so forth. The electron flux for a given channel (e.g., second and third lines in Table 1) is multiplied by the calculated energy channel width to provide the electron flux of that channel in 1/(cm^2 sr sec).

Table 1: An example of an electron energy spectrum input file

0	0.5	1	2	5	10	20
100	3.67E+04	4.21E+03	4.83E+02	5.55E+01	6.37E+00	7.31E-01
150	7.34E+04	8.42E+03	9.66E+02	1.11E+02	1.27E+01	1.46E+00

3.4.3 Electron Beams. If the user desires to model a normally incident beam with a spectrum of energies, the number of angular bins in AF-NUMIT2 must be set to one. After that, the input file is prepared in almost the same way. The difference is that the electron flux for each channel will be in 1/(cm^2 sec MeV) because the steradian units are meaningless for a beam. For mono-

[6] We use parenthesis to identify the parameter name that appears in the actual AF-NUMIT2 code.
[7] A provision does exist in the code to make this calculation logarithmic. That is, the width is calculated from the natural log of the energy distance to the channels on either side.

energetic beams, only one energy channel and flux should be given in the comma-delimited input file. In that case, the electron beam flux will simply be 1/(cm^2 sec).

3.5 Provisions for Time-sequenced Incident Electron Flux Environments

AF-NUMIT2 can easily handle a changing energy spectrum electron flux environment. In the comma-delimited input file additional rows are added for new electron fluxes. The first cell in each row designates the time in seconds that that flux will be incident. In the example of Table 1 these values are 100 seconds for the first spectrum and 150 seconds for the second. The other cells in each row indicate the electron flux for the corresponding energy channel. In the Table 1 example, the second electron flux for each energy channel happens to be twice that of the first. The energy spectrum loop will be run for each electron flux energy spectrum (i.e., each row past the first row in the energy spectrum input file). Once the dose rate and initial current profiles are determined, the transport code in the time loop will track the movement of charges for the designated length of time—in the example 100 and then 150 seconds. During this time, the model continues to simulate the input of additional electrons and energy as specified in the input file. At the end of the simulation time for an electron flux energy spectrum, the final resulting electric field, charge distribution, and current profile—as determined during the time loop—are stored for plotting. The dose rate used as determined by BeeckenTabFred is also stored. In the example, plots would be made representing the situation at 100 seconds and 250 seconds.

If the user does not desire to change the incident electron flux environment, but wishes to track the development of the calculated parameters in time, then in the .csv input file the user puts the same flux in multiple rows. An updated plot will be made of each parameter after the time chosen for each row is completed.

It is important to note what the AF-NUMIT2 model does when changing from one electron flux energy spectrum to the next (one row to the next in the input file). The only carry-over from the previous electron flux is the position dependent charge deposition profile (rho). The dose rate profile (Dose) starts over for the new flux, in keeping with the thinking that radiation induced conductivity “RIC” has no persistence or time dependence (see Section 3.8). Obviously a new calculation must be made of the initial current (Jo) because it is due solely to the incident electrons. The charge induced on the electrodes is recalculated on every trip through the Time Loop and is based solely on the charge that is deposited within the dielectric. The electric field is also calculated each trip through the Time Loop and it is based solely on the deposited charge and the charges induced on the electrodes.

3.6 Extension of Model for Incident Electrons to Lower Energy Range

A significant limitation of NUMIT to be addressed in the present work was its restriction to modeling only incident electrons with energies greater than 100 keV. In the space environment there are normally significant fluxes of electrons at lower energies, and these are believed to make important contributions to the deep dielectric charging problem. There is nothing inherent in the transport model part of NUMIT that excludes the use of lower energies. However, as published, both the energy deposition algorithm EDPOS [3] and the charge deposition model FredBell [4] are only valid for incident electron energies 0.1–20 MeV.[8] The task then is to extend EDEPOS and FredBell to lower energies or to replace them.

3.6.1 A Lower Incident Energy Model. An important effort has been made by a group at JPL to address the limitations of EDEPOS. [18] Kim et al. did Monte Carlo electron transport calculations using TIGER/ITS3. They observed that for a given material, with incident energies 10–100 keV, the energy dose profiles all have the same shape and "can be reduced to a single curve by normalizing them using energy dependent scaling factors for the depth and the energy deposition."[9]

Naturally, the total of all deposited energy must be dependent on the incident energy. Accordingly, Tabata and Ito [3] showed that the integral of the dose D is proportional to the incident energy T_0,

$$\int_0^\infty D(x)\,dx = fT_0,$$

where f is a normalization factor that accounts for the fraction of incident energy backscattered from the surface and the energy deposited deeper due to the bremsstrahlung tail. Implicit in this formulation is the use of x as depth from the surface of the material written in terms of g/cm^2.

Commonly, the depth is converted to normalized depth $w = x/R_{ex}$, where R_{ex} is the extrapolated range of the incident electrons for a given material and energy. Kim develops a normalized dose profile $g(w)$ and relates it to the actual dose profile through a vertical scaling factor S_y:

$$D(x) = S_y\, g(w).$$

[8] Frederickson does provide tables that allow for interpolation of FredBell up to 100 MeV.
[9] Frederickson suggested to this author in 2000 that we ought to be able to make a reasonable approximation of the dose profiles at lower energies by scaling down from a higher energy using the incident energy ratio and the ratio of extrapolated ranges. Kim's detailed work validates this approximate approach.

Kim found an equation for the normalized dose profile $g(w)$, but does not provide the necessary fitting parameters. Nevertheless, we can make progress because Kim has validated the scaling principle.

For the specific case of 100 keV incident energy electrons the EDEPOS algorithm claims validity. Thus, we choose $D(x) \rightarrow D_{100}(x)$. In addition, because Kim's $g(w)$ is valid for the incident energy range 10–100 keV, we can also write the following expression for $D_{low}(x)$ at all incident energies in that range lower than 100 keV:

$$D_{low}(x) = S_{y_{low}}\, g(w).$$

By combining these last two equations we can eliminate Kim's normalized dose profile:

$$D_{low}(x) = \frac{S_{y_{low}}}{S_y}\, D_{100}(x).$$

Kim shows that

$$S_y = \frac{f\, T_0}{R_{ex}}.$$

Therefore, for incident energies lower than T_0 = 100 keV, we can also write:

$$S_{y_{low}} = \frac{f_{low}\, T_{0_{low}}}{R_{ex_{low}}}.$$

By substitution we now have an expression that converts a dose profile at 100 keV to a dose profile at lower energies:

$$D_{low}(x) = \left(\frac{f_{low}}{f}\right)\left(\frac{T_{0_{low}}}{T_0}\right)\left(\frac{R_{ex}}{R_{ex_{low}}}\right) D_{100}(x). \tag{4}$$

Using their Monte Carlo simulations over the incident energy range 10–100 keV, Kim finds values for *f*, an equation for R_{ex}, and a functional fit for the normalized dose profile $g(w)$. Clearly, this is a significant step forward, and Kim demonstrates how very precisely the formulation fits some of the Monte Carlo simulations. Unfortunately, two fitting parameters are required for R_{ex} and six more fitting parameters are required for $g(w)$. Although graphs of these parameters were published, no equations for the parameters were found. In addition, the normalization factor *f* was presented as a three-dimensional plot with the proposal that a simple fitting function, requiring four more fitting parameters, may be developed that could be used instead of their plotted *f*.

3.6.2 Implementation in AF-NUMIT2. For the purposes of extending AF-NUMIT2 to lower energies, the work by Kim is enormously helpful. However, with a total of twelve fitting parameters required, none of which has an equation provided, it is clear that the degree of precision of the work done by Kim could not be readily adapted to AF-NUMIT2. Nevertheless, the basic idea represented by Equation (4), derived from our analysis of Kim's work, provides a path to an approximation without the necessary fitting parameters.

Tabata [3] [19] claims a region of validity for his algorithm for extrapolated range R_{ex} down to about 0.3 keV. His algorithm for the normalization factor f is said to be valid down to 50 keV. Furthermore, Kim [18] reports that comparison of their f with Tabata's f down to 10 keV yields a deviation within ±4 %. Thus, using Tabata's algorithms, we can calculate two of the three factors in Equation (4). The third factor is a simple ratio of incident energies. All that remains for an approximation of the dose profile $D_{low}(x)$ below 100 keV is a good profile for *D(x)* at 100 keV. Tabata's EDEPOS is claimed to be valid down to 100 keV, so that algorithm fills the requirement.

The BeeckenTabFred algorithm for charge and energy deposition profiles branches at T_0 = 100 keV. If the incident energy is at or above 100 keV, then a streamlined, combined version of EDEPOS and FredBell is used. If, however, the incident energy is below 100 keV, then the low energy branch is utilized. In this branch, the profiles at 100 keV are calculated first. Then, Equation (4) is used to scale the vertical axis of the Dose, corresponding to the energy deposited. The depth or horizontal axis is scaled by $R_{ex_{low}}/R_{ex}$, which is consistent with the normalized depth *w* utilized by Kim and many others.

What about the electron deposition? The FredBell algorithm provides a profile of the incident current as it drops to zero. To find electron deposition from it, the user simply takes the derivative. Therefore, when scaling to lower than 100 keV, there is no reason to adjust the vertical scale. We simply take the derivative and scale the horizontal axis in the same manner as for the Dose.

3.6.3 Results of new Lower Incident Energy Model. Figure 5 shows the results of Kim's dose profiles determined by Monte Carlo calculations (the only profiles provided using incident energies below 100 keV). [18] In Figure 6, the profiles were found using the approximation of

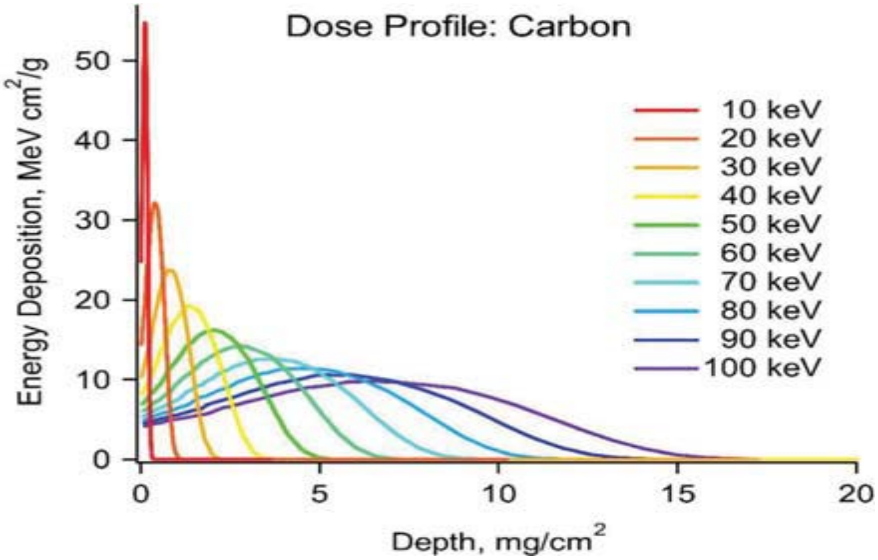

Figure 5. Incident energy deposition plot made by new JPL algorithm and Monte Carlo work

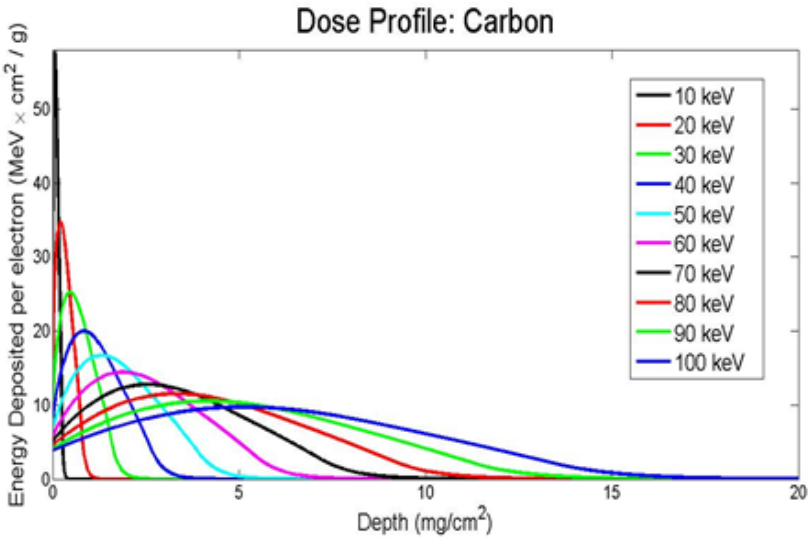

Figure 6. Incident energy deposition plots made by BeeckenTabFred approximate algorithm

the BeeckenTabFred algorithm. Although similar, the two profiles for normal incidence are not the same. The peaks are surprisingly close in magnitude, but the approximate algorithm method has the peaks forming slightly closer to the surface than the Monte Carlo calculations. Why the difference? There are four possibilities:

1. The factor f_{low} used in the approximate algorithm is Tabata's, and it is not claimed to be valid below T_0 = 50 keV.
2. The algorithm uses R_{ex} as determined by Tabata, which although according to Tabata is valid in the range plotted, is not the same extrapolated range as used by Kim.
3. Kim does not provide the density for the carbon used, and since carbon has a range of densities, the value used in our algorithm was simply a guess.
4. The algorithm requires a good fit by EDEPOS at 100 keV because that is the dose profile that is scaled to all the lower energies.

The first possibility would seem to be an obvious problem. However, Equation (4) only scales the height of the dose rate curve, not the shape. Therefore, since f_{low} is only used by the BeeckenTabFred algorithm in the context of Equation (4), it cannot be the problem.

In the second possibility, the extrapolated range R_{ex} is utilized by BeeckenTabFred in two ways. First, it is used in Equation (4), which we have already shown cannot be the issue. Second, it is used to scale the horizontal axis by $R_{ex_{low}}/R_{ex}$. This could be a problem, but Tabata claims R_{ex} is valid to energies way below those considered here (~0.3 keV). Therefore, it would seem unlikely the discrepancy comes from this source.

For the third possibility, if different values of density were chosen for carbon, the problem is specific to this case. The BeeckenTabFred algorithm was run for carbon with densities of 1.8 g/cm^3 and 2.26 g/cm^3 (and even the unrealistically extreme case of 0.8 g/cm^3). The results were identical—not unsurprising because the Depth (mg/cm^2) indicated by the horizontal axes in Figure 6 is scaled by the density.

The fourth and last possibility remains. Without any real doubt, the discrepancy between Tabata's EDEPOS algorithm at T_0 = 100 keV and Kim's Monte Carlo result is the cause of the differences observed between Figure 5 and Figure 6. The 100 keV line in the lower plot comes directly from EDEPOS because that falls within the validity range. Note it peaks at about 5.5 mg/cm^2 and the equivalent line in the upper JPL plot peaks at about 7 g/cm^2. When scaling the horizontal axis to lower energies, this difference will be propagated. As discussed in the next section, there is reason to believe that the JPL algorithm by Kim is better than EDEPOS at T_0 = 100 keV.

3.7 Verification of the Energy Deposition Model in NUMIT

In order for AF-NUMIT2 to be useful, the depth profiles for the deposition of the incoming electrons and their energies must approximate reality. As discussed earlier, Tabata and Frederickson used limited experimental data and Monte Carlo simulations to develop algorithms

that describe these depth profiles for various materials. Because these algorithms were only designed to be valid for incident electron energies above 100 keV, the last section was devoted to describing the present attempt (the algorithm BeeckenTabFred) to extend the profiles to lower incident energies. But how valid is this attempt, and for that matter, how valid are the original algorithms?

In fact, why bother with the approximate algorithms? Why not run a Monte Carlo simulation for any situation to be modeled by AF-NUMIT2? Monte Carlo can be used to track the deposition of energy and charge in the dielectric and from this we can produce energy dose and charge deposition depth profiles. Unfortunately, even on modern computers, Monte Carlo simulations often take hours to run and require being redone for every incident electron energy and/or change of material. Such an approach is impractical for modeling the simultaneous incidence of a wide energy spectrum of electrons—the reason NUMIT is being redesigned. More importantly, AF-NUMIT2 is a tool for investigating various factors—materials, conductivities, temperatures, flux spectra, and combinations of flux spectra—in an effort to determine what conditions make electrostatic discharge likely. There are so many possible combinations of parameters that slow processing would make such investigations unwieldy.

Because the BeeckenTabFred algorithm is based on prior work, we believe it should be sufficiently accurate, but the only known basis of comparison is one graph published by JPL [18] for energy deposition in the material carbon (reproduced in Figure 5). The goal here then is to produce Monte Carlo simulations that will be able to determine the efficacy of the extended algorithm. Hopefully, this simple, fast algorithm will at least approximate the energy and charge deposition profiles in various materials at lower incident electron energies.

3.7.1 Setup of the Monte Carlo Method. MCNP6 Beta Version 2 was used to run Monte Carlo (MC) simulations to find the energy and charge deposition profiles in different materials with incident electron energies between 10 and 100 keV. In order to run a simulation using MCNP6, input files need to be created with the correct problem and geometry setup. The material is divided into many surfaces, all stacked up in series with a small “segment” in between each surface. MCNP6 fires electrons at the resulting mesh. The segment width can be varied as necessary to produce the desired resolution of the energy curves. More surfaces with smaller segments in between construct a finer mesh which will in turn result in greater resolution—important particularly for the sub 50 keV energies. However, more surfaces also greatly increases the computation time for the simulation so that a coarser mesh must be used at higher energies where greater penetration depths are modeled. The cell is comprised of a single material which is defined by the effective atomic number, the effective mass number, and the material density. The total energy per gram deposited in each segment is tallied by MCNP6 and written to an output file.

After the geometry of the problem is set up, the electron source needs to be defined. For these MC simulations we sent one million electrons into the material and MCNP6 tracked their movement and the deposition of their energy within the mesh. Once an electron deposits its energy and is left with 100 eV or less, the tracking stops. Monte Carlo simulations were run for a few different materials, calculating both the energy and charge deposition. They are described below.

3.7.2 Examination of Low Energy Algorithm for Energy Deposition. Monte Carlo simulations of energy deposition have been published for carbon by JPL and were reproduced in Figure 5 along with our extended BeeckenTabFred algorithm results in Figure 6. As a baseline, we ran MNCP on the same situation. Figure 7 is the result of MC simulations produced by David Dixon, a graduate student at the University of New Mexico who introduced us to MCNP. Using what we learned from Dixon, we were able to produce a similar result, Figure 8 for carbon (Z=6, A=12, ρ=2.1 g/cm^3). Comparison of Figures 5, 7, and 8 shows the similarity between the three Monte Carlo plots. The peaks are all in the same place, although of slightly different heights. The differing heights are apparently due to subtle differences between versions of MNCP6 and the TIGER/ITS3 used by Kim at JPL. We used beta version 2 on our plot, but we have also used identical inputs to compare the results to beta version 3 and found the resulting vertical scales to be different. We are not sure what version David Dixon used for his plot, but we believe it was MCNP5. Regardless, the main purpose here is to verify the shape of the dose curve.

As mentioned at the end of Section 3.6, the peaks of the dose in the extended algorithm plots of Figure 6 are about 20 % closer to the surface than the MC plots. Since the MC plots of Figures 5,

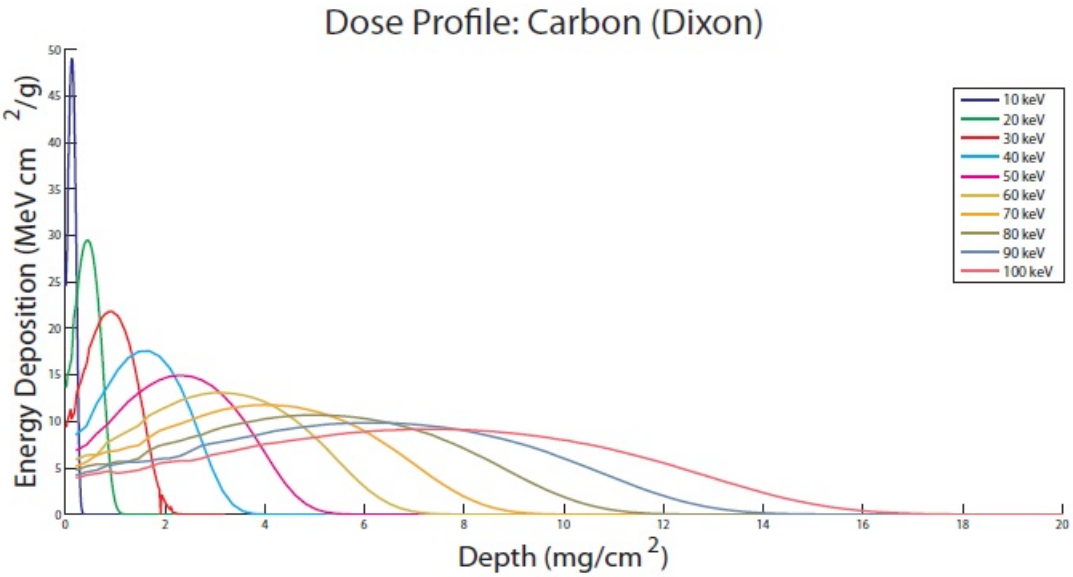

Figure 7. Monte Carlo simulations of normal incidence on Carbon by David Dixon

7, and 8 are all consistent, it looks bad for our extended algorithm. However, the difference holds true for the 100 keV case which is *not* part of the extended algorithm but a result of the original EDEPOS algorithm. Thus, it seems that the EDEPOS algorithm at 100 keV is not as accurate as Kim's algorithm which he fit to their MC simulations at 100 keV. It would be interesting to

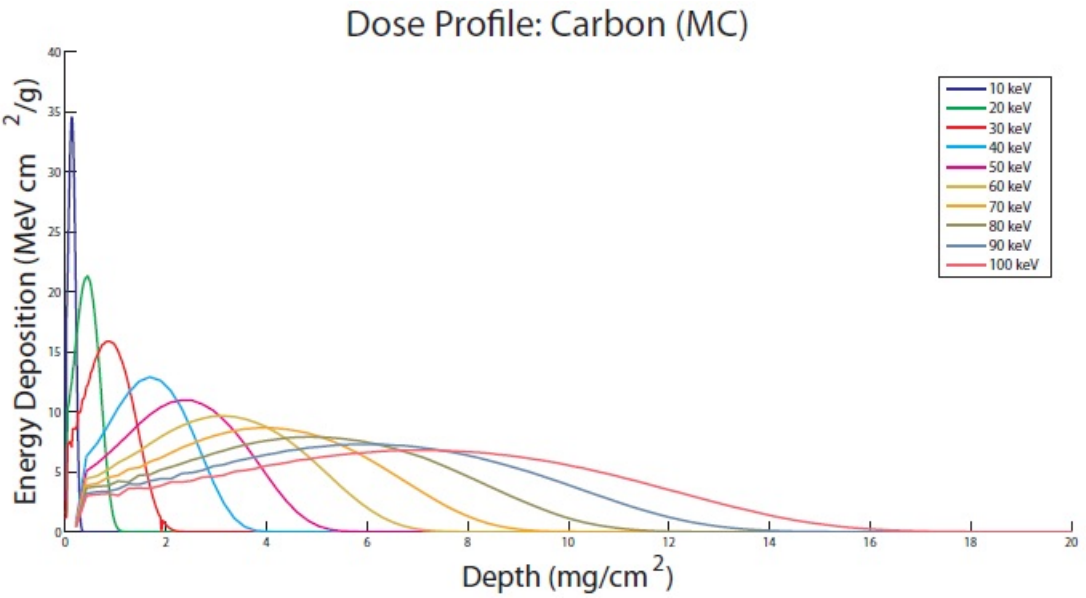

Figure 8. Monte Carlo simulations of normal incidence on Carbon

follow this difference between modern MC results and EDEPOS through to higher energies and in different materials. Time, however, is a limiting factor and EDEPOS has been thought for decades to be sufficiently accurate for modeling purposes.

Teflon was the second material that was used to compare MC simulations with the new BeeckenTabFred algorithm. Energy deposition curves were produced with MCNP for incident electron energies from 10 to 100 keV in increments of 10 keV, see Figure 9. In this case, the same segment width of 1.0 μm was used in the geometry setup for most energies, although smaller segments were needed for the lower energies of 10–40 keV.

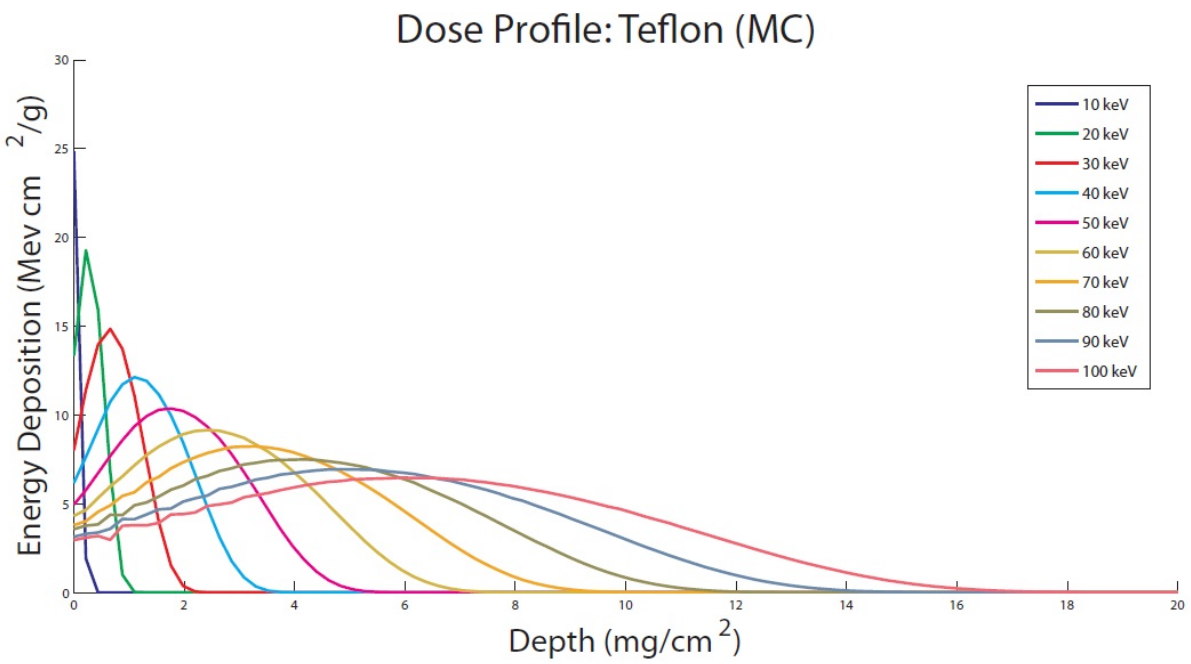

Figure 9. Monte Carlo simulations of normal incidence on Teflon

The BeeckenTabFred algorithm was then run for Teflon using the effective atomic number 8.28 and effective atomic weight 17.25 with mass density 2.2 g/cm^3, see Figure 10. The results shown in Figure 9 and Figure 10 are quite similar, but in order to get an accurate picture of the differences, individual energy curves must be plotted on the same graph as shown in Figure 11

The BeeckenTabFred algorithm, which for this energy identical to EDEPOS, is slightly offset to towards the surface compared to the MC results.[10] It is clear that the EDEPOS algorithm predicts a slightly shallower deposition of energy at 100 keV than our current MC simulations show. Because BeeckenTabFred is a scaling of the 100 keV case, this slight offset propagates to the rest of the energies that were compared for Teflon and carbon.

Figure 12 provides further comparisons between MC simulations and the BeeckenTabFred algorithm that extends EDEPOS to lower energies. Although the mesh size for the 20 keV case was apparently too coarse for good results, it appears again that the MC simulations are indicating slightly deeper energy deposition compared to the algorithm—consistent with expectations based on the difference at 100 keV.

[10] The results from the MC simulation were vertically scaled by a factor of 1.47 in order to more effectively compare the two deposition curves. Vertical scales are difficult to correlate in this type of modeling. At this point in the research, the shape of the distribution is of primary concern. Furthermore, we have observed that performing exactly the same simulation with beta versions 2 and 3 of MCNP6 resulted in different vertical scales.

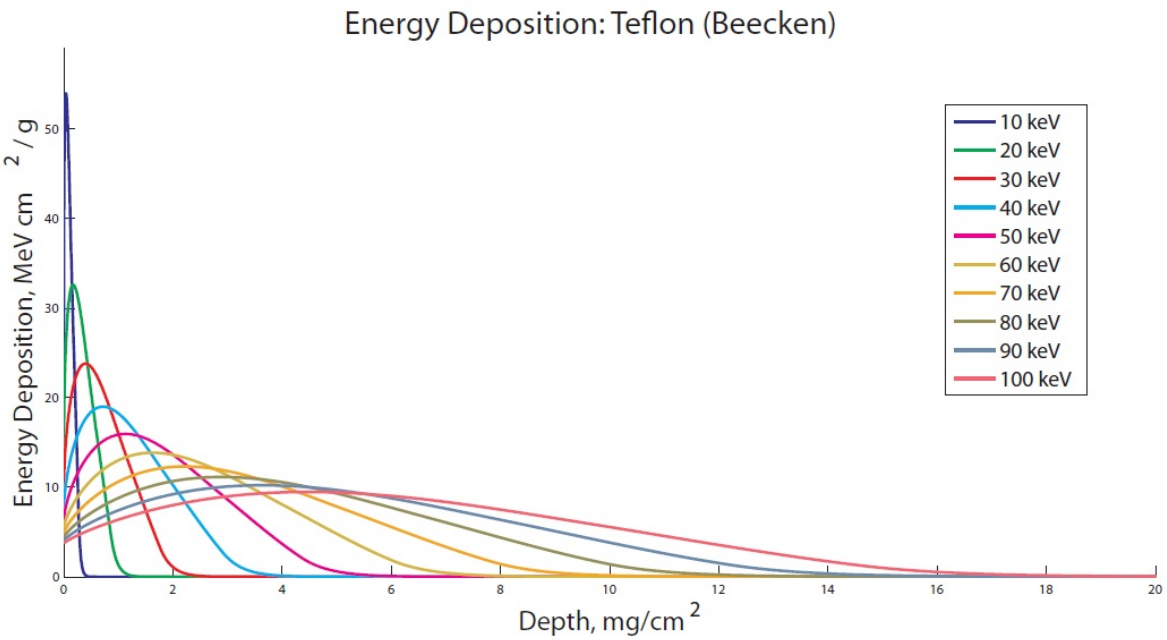

Figure 10. Results of BeeckenTabFred algorithm for normal incidence on Teflon

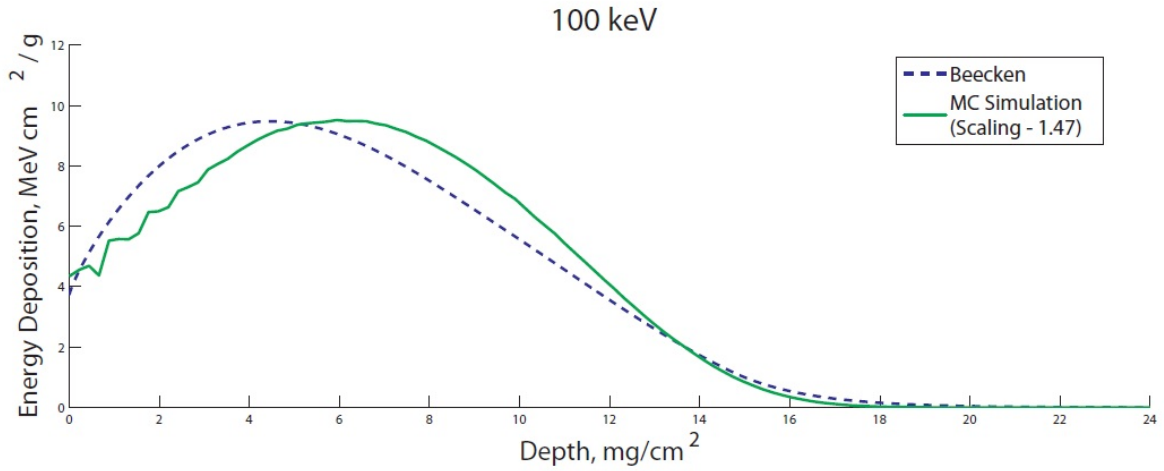

Figure 11. Comparison of BeeckenTabFred algorithm with MC simulation

The slight ripple of the MC curve in Figure 11 for 100 keV was investigated in order to determine whether or not the mesh size was the issue. The "stair step" nature of the graph would seem likely to be caused by simulating a continuous process with a discrete algorithm, therefore the MC simulation was repeated for Teflon with 100 keV incident electron energies but with the mesh size cut in half from the previous simulation run. The two curves have the same ripple, and the smaller mesh size did not improve the resolution of the curve. Perhaps an even smaller mesh would succeed in eliminating this effect, but this seems unlikely. Another possible solution

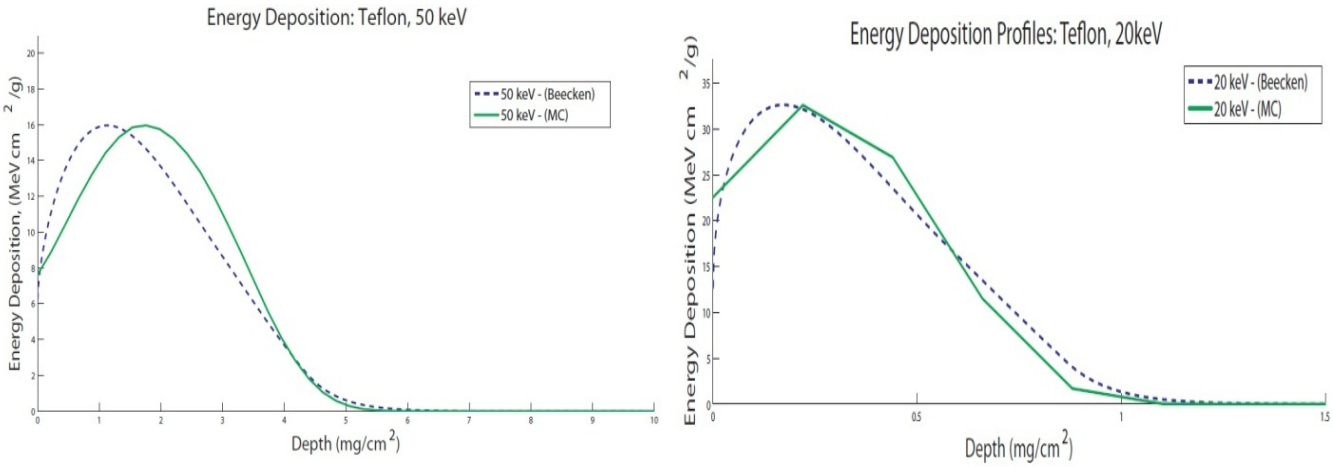

Figure 12. Detailed comparisons of algorithm with MC at 50 and 20 keV.

would be to run the MC simulation again with many more incident electrons. Similar ripples show up in Dixon's independent results in Figure 7.

Comparisons between Monte Carlo simulations and the BeeckenTabFred algorithm were also made for aluminum which has greater atomic number (13), atomic weight (27), and density (2.7 g/cm^3). The results showed the same trend identified above.[11]

3.7.3 Examination of Low Energy Algorithm for Charge Deposition. Although it was *not* part of the statement of work, it is important to also investigate the validity of the BeeckenTabFred algorithm in terms of charge deposition. Monte Carlo simulations were performed at energies between 10 keV and 100 keV for carbon, Teflon, and aluminum. For aluminum, we looked only at where the electrons stopped due to the material stopping effect and inferred a current from that. Effectively, this makes the aluminum non-conducting for the purposes of the simulation, but aluminum is such a standard reference material for radiation shielding it was an appropriate choice.

Figure 13 illustrates the results for aluminum (non-conducting) at 100, 50, and 10 keV. As expected from the energy deposition results, the electron depositions from the algorithm were slightly closer to the surface for 100 and 50 keV. Surprisingly, the 10 keV case had MC depositing the electrons closer to the surface. The result is interesting because for carbon and Teflon the trend had held. Probably, what is really being indicated by these differences is that the approximations made by the algorithm worsen as the extreme low energy of 10 keV is approached.

[11] The results of these comparisons are documented more thoroughly in the 21 Month After Award report.

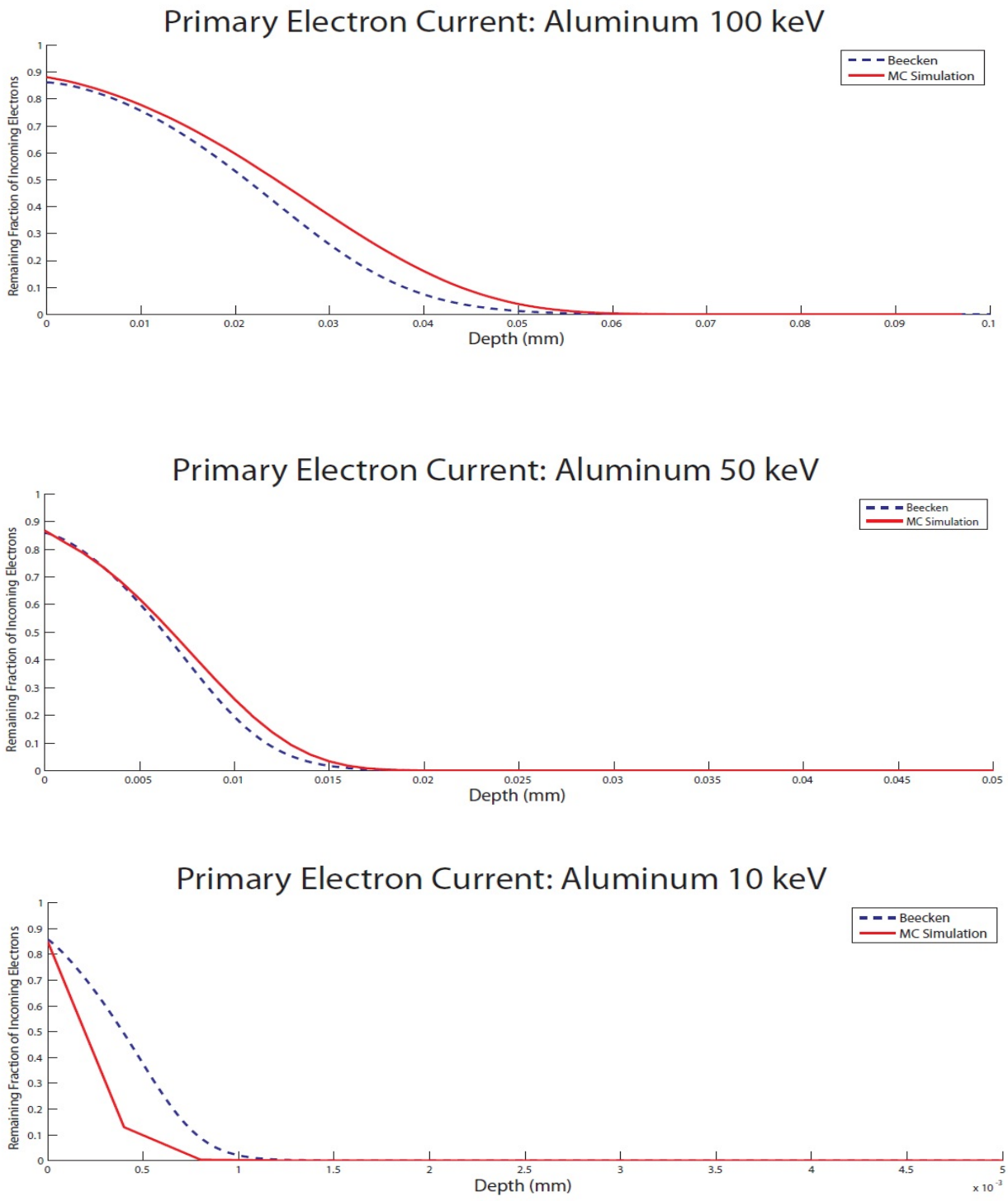

Figure 13. Comparisons of electron deposition results: BeeckenTabFred algorithm vs. Monte Carlo simulations

3.7.4 Examination of Algorithms for Isotropic Incidence. The goal in redesigning NUMIT into a tool useful for modeling the spacecraft environment necessarily included accounting for electron incidence at various angles other than perpendicular to the surface. The method chosen was described in Subsection 3.3.2. In an effort to test the validity of the method, we ran MC simulations for a large number of circumstances. This task is rather involved because there are so many factors. We used MCNP6 Beta Version 3 for incident energies of 10, 20, 50, 100, 200, 500, and 1000 keV on carbon and aluminum. Angles used were 0º, 30º, and 60º. Results were found for both energy and charge depositions. All totaled, for all of these possible combinations, there would be 84 plots. We ran 82 of them, requiring hundreds of hours of computation time.

The sheer volume of results was somewhat overwhelming, but some general observations can be made. Many of the MC simulations were very similar to the algorithm. Normally, the peaks were relatively close. The similarity deteriorated as the angle from the normal was increased. However, due to enhanced backscatter at greater angles there are fewer electrons entering the material at these angles. Therefore the discrepancy is less of a problem.

Unfortunately, this effort at validation was very time consuming and not really conclusive. It did seem to indicate strongly that the algorithm approach being taken is valid as a first order approximation. In retrospect, however, some things should have been done differently. First, given the difference in energy deposition quantities between MCNP6 Beta Version 2 and Version 3, it would have been better to use MCNP5 or wait until MCNP6 was finalized. Secondly, the algorithm runs that were plotted as comparisons on the same graphs were not done with backscatter accounted for in the algorithm. Since MCNP does take backscatter into consideration, the comparisons on the vertical scales (energy or number of electrons deposited) were compromised from the start. This inherent difference in the basis of comparison will be more of an issue at greater incident angles which have more backscatter—precisely where the discrepancy increased.

Further consideration of the problem has resulted in the conclusion that the accuracy of the algorithm approximation for a single angle is not only inconsistent, but it is really not the important comparison. Since it is isotropic fluxes that are being modeled, the only thing that really counts is how the result—after summing through all the possible angles—compares with reality. Thus, the appropriate approach is to do Monte Carlo simulations with isotropic incidence of electrons instead of using a beam set at various angles.

Some preliminary Monte Carlo studies of isotropically incident electrons have been done in collaboration with David Barton of AFRL/RVB. Barton used MCNP5 to simulate isotropic electrons incident on aluminum at various energies. These simulations included backscatter of electrons off the surface. The electron deposition profiles for five different incident energies are

plotted as points in Figure 14. The solid lines in the figure are the results of the BeeckenTabFred algorithm (with the backscatter feature on) used in AF-NUMIT2.

Barton also found the energy deposition profiles in aluminum with MCNP5 for the same incident energies of isotropic fluxes. The results of both the algorithm and the MC simulations were put on the same scale with the same units and plotted in Figure 15. The points are MC simulation data and the solid lines are the AF-NUMIT2 deposition algorithm.

Although it might appear that the correlation between the MC simulations and the algorithm is not impressive, never before have MC simulations been used to find depth profiles of charge *and* energy deposition for isotropically incident electrons of several energies. Furthermore, no algorithm besides BeeckenTabFred is known to exist that estimates deposition depth profiles from isotropic incidence, much less for a large range of materials and energies. This algorithm was developed without the aid of MC simulation or lab data—it is the result of an analytical

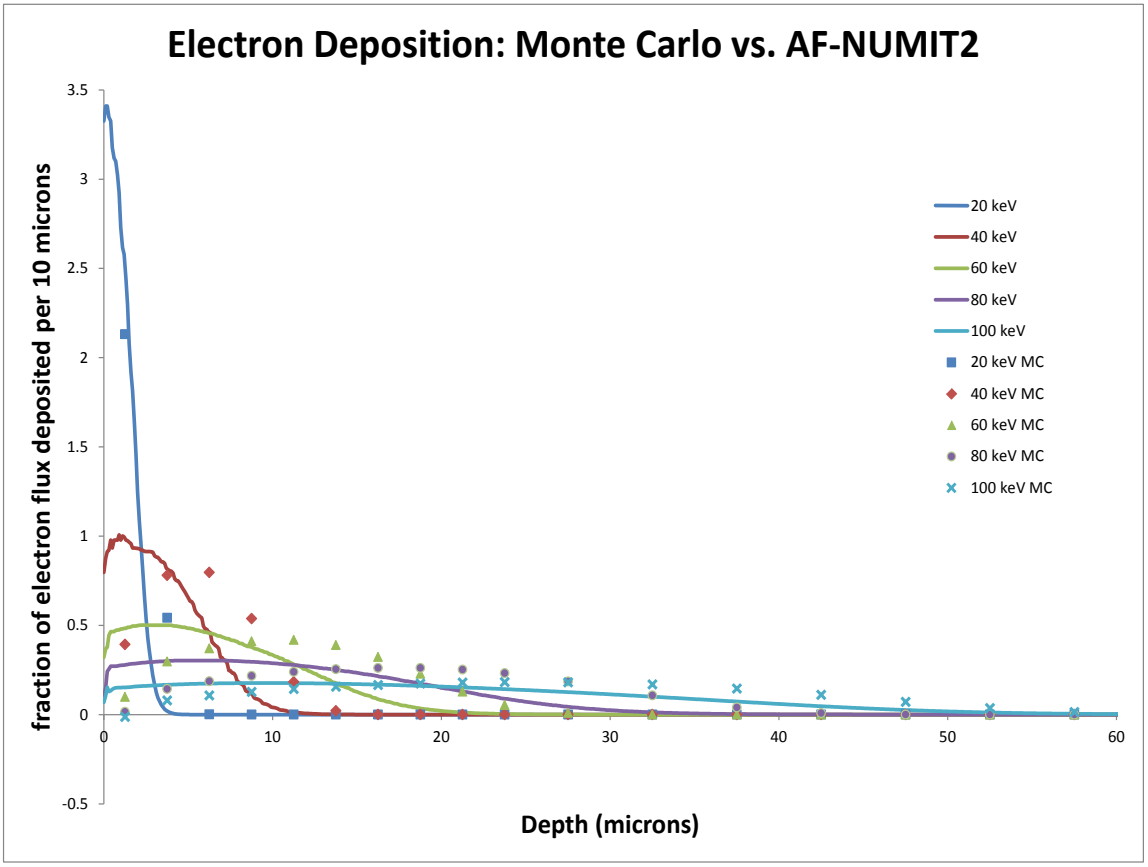

Figure 14. Monte Carlo simulations of electron deposition vs. BeeckenTabFred algorithm for isotropically incident elctrons on aluminum

extension of a normal incidence algorithm. The fact that these two independent results have a

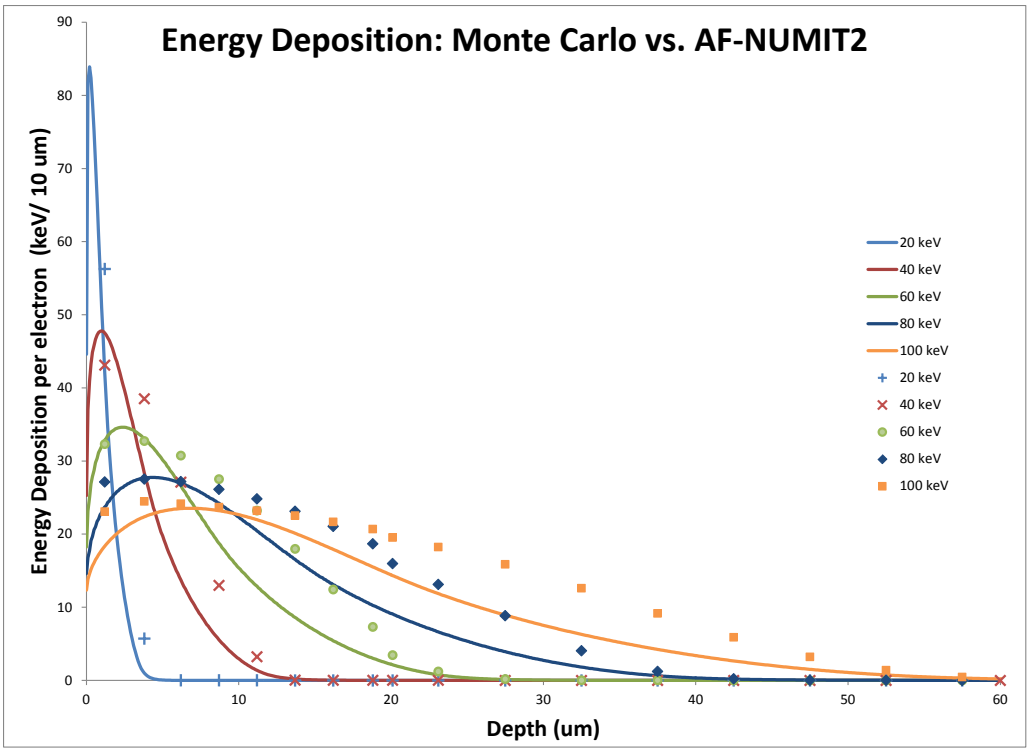

Figure 15. Monte Carlo simulations vs. BeeckenTabFred algorithm for isotropically incident electrons

worst case discrepancy that only in some places approaches 50 % is remarkable. Given the other uncertainties involved with deep-dielectric charging in spacecraft, it would seem that the algorithm is an appropriate approximation. At the same time, these results provide a clear path forward. Monte Carlo simulations of isotropic incidence need to be made for a wide range of energies on a large selection of materials. Then, a better algorithm might possibly be developed to insert into AF-NUMIT2.

3.8 Development of Time-Delayed and Temperature-Dependent Radiation Induced Conductivity Algorithms

Development of time-dependent RIC and temperature-dependent RIC algorithms were originally thought to be an important part of this work. However, during a 25 July 2012 meeting at AFRL/RVBX, these parts of the original proposal were reconsidered. Some at the meeting characterized such algorithms as relatively unimportant compared to the other goals. Another participant raised the possibility that including such features might be dangerously misleading. Users might come to believe that AF-NUMIT2 is correctly accounting for temperature and time dependence, when at best the simulation could not be more than a guess.

In the case of temperature dependence, it is very clear that there can be a significant effect. Ferguson et al. [20] have shown experimentally that conductivities can change by orders of magnitude with temperature. However, the lack of sufficient data over a wide enough range for important materials is a major obstacle to creating an algorithm. As regards time dependence, although there exist clear possible approaches to an algorithm that includes this effect, it is almost impossible to find the time constants required for such models.

After much discussion, the consensus was that if AF-NUMIT2 users wish to incorporate temperature affects, this would be best done by simply having the users input the RIC coefficients and dark coefficients that they believe exist at the temperatures they desire to model. Changing those coefficients as the simulation progresses is rather easily accomplished, and that would give the users complete control of their temperature modeling.

4.0 RESULTS AND DISCUSSION

4.1 Preliminary Simulation Results

In order to test AF-NUMIT2, we obtained preliminary results by running it extensively with realistic electron flux energy spectra. Figure 16 shows various spectra obtained by CRRES that were downloaded and formatted into input files suitable for the simulation.[12] These data were used in a variety of combinations as inputs to AF-NUMIT2 in order to predict the maximum electric field within Kapton after at least 8 days of exposure—sufficient time in almost all cases for equilibrium to be achieved. The simulations normally took about two minutes to run for each simulated day.

[12] The author is grateful to W. Robert Johnston of AFRL/RVBX for assistance. The data were obtained in two overlapping sets during each minute of collection. These data are available at ftp://virbo.org/users/johnston/crres.

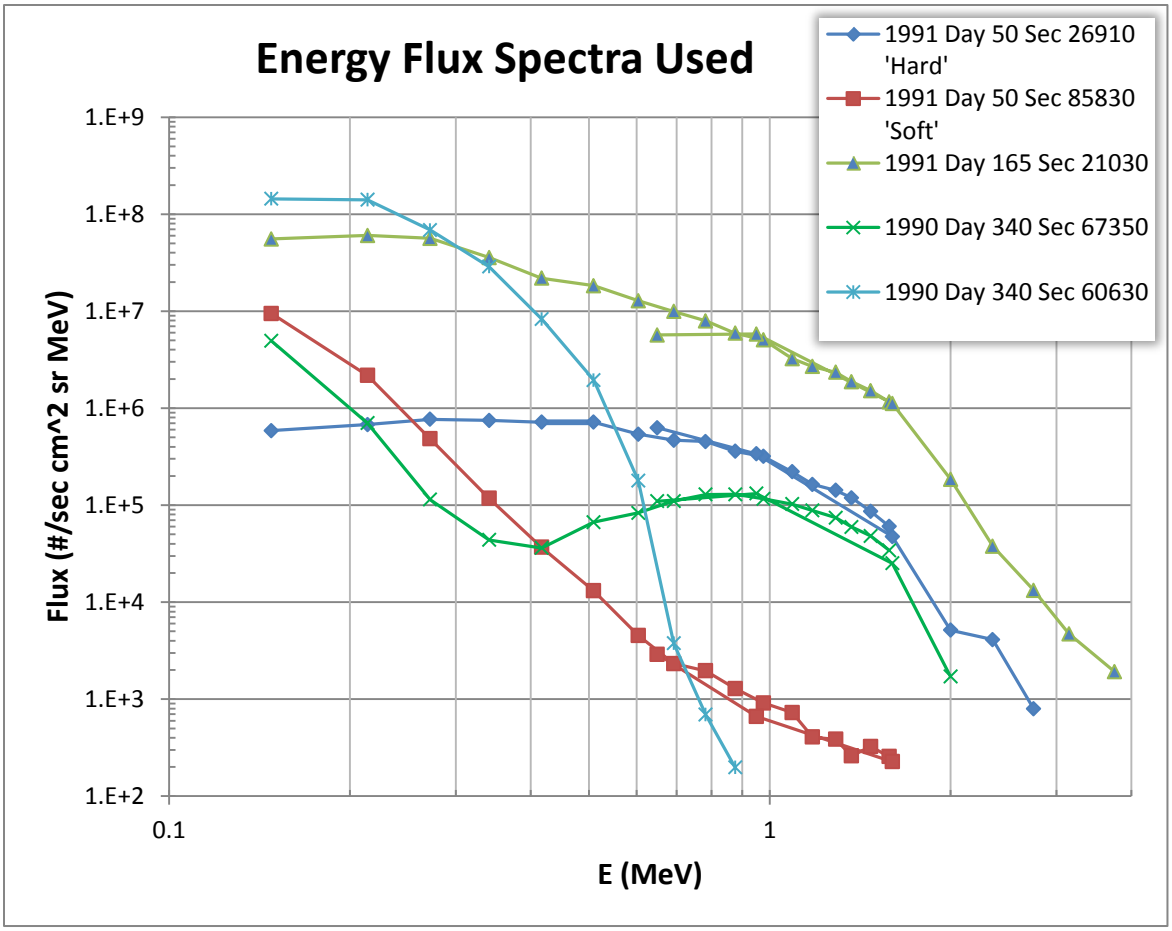

Figure 16. CRRES data used to run simulations in AF-NUMIT2

A wide range of possible values exist for the dark conductivity and RIC coefficients in Kapton.[13] Dark conductivities might be as high as 6×10^{-20} or as low as 4×10^{-25} 1/(Ω cm). The possible RIC coefficients have almost as large a possible range, from 5×10^{-16} to as low as 5×10^{-18} (sec/(Ω cm rad)). Figure 17 shows the results of a simulation with AF-NUMIT2. In this simulation, four days of the "hard" spectrum from Figure 16 were run, followed by four days of "soft" spectrum. For all 8 days we used a dark conductivity of 7×10^{-22} 1/(Ω cm) and a RIC coefficient of 4.5×10^{-16} (sec/(Ω cm rad)). Each day is plotted as a separate line in these graphs. Because equilibrium was essentially achieved for the "hard" spectrum after one day, all four days are plotted on top of each other. Then the spectrum shifted to "soft" for the remaining for plots corresponding to the situation at the end of each day's simulation. The dose rate, or energy deposition curves, clearly reflect these two different input spectrums. The electron current profile is always flat, indicating

[13] Data provided in private communication with JR Dennison of Utah State University.

equilibrium was achieved after one day for both spectra. The maximum electric field did not approach the typical risk level for discharging (10^5 V/cm) before equilibrium was reached at the end of the first day, at the end of four days, or at the end of the total eight day simulation. In fact, based on this simulation, there appears to be no chance of discharge-level electric fields being reached.

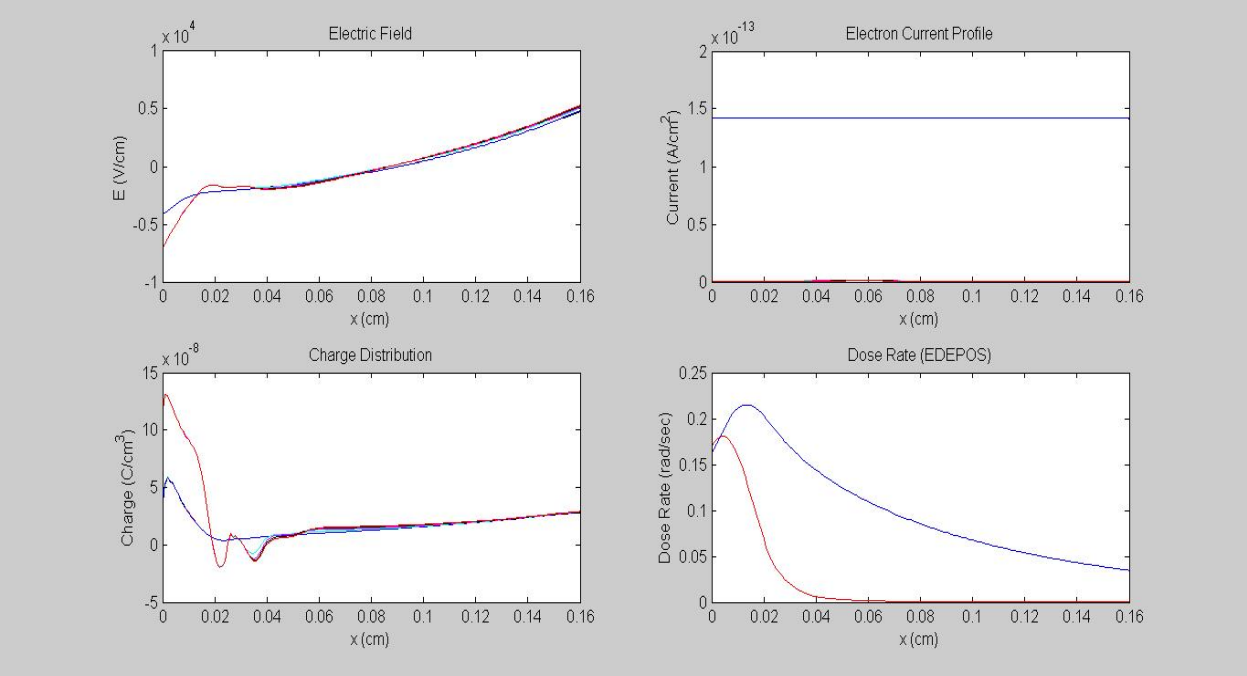

Figure 17. AF-NUMIT2 simulation results after 4 days of "hard" and 4 days of "soft"

Both of the conductivity values in this simulation were at the high end. We would expect high conductivity to lead to larger bleed-off of deposited charge. Therefore, it becomes appropriate to explore the entire range of conductivites. Over thirty simulation runs were made with various combinations of incident energy spectra, dark conductivities, and RIC conductivity coefficients. Displayed in Figure 18 are the results of a simulation run made with the same hard-soft energy spectra over the same number of days. This time, however, we chose to decrease the RIC coefficient by two orders-of-magnitude to 5×10^{-18} (sec/(Ω cm rad)), at the low end of the possible value range. The dark conductivity was also increased by two orders-of-magnitude to 7×10^{-20} 1/(Ω cm), but there is reason to believe that this did not affect the results. During the eight days, the simulation did not reach equilibrium. Instead the electric field increased until it reached approximately 4.4×10^5 V/cm, beyond the electric field strength commonly understood to cause discharge.

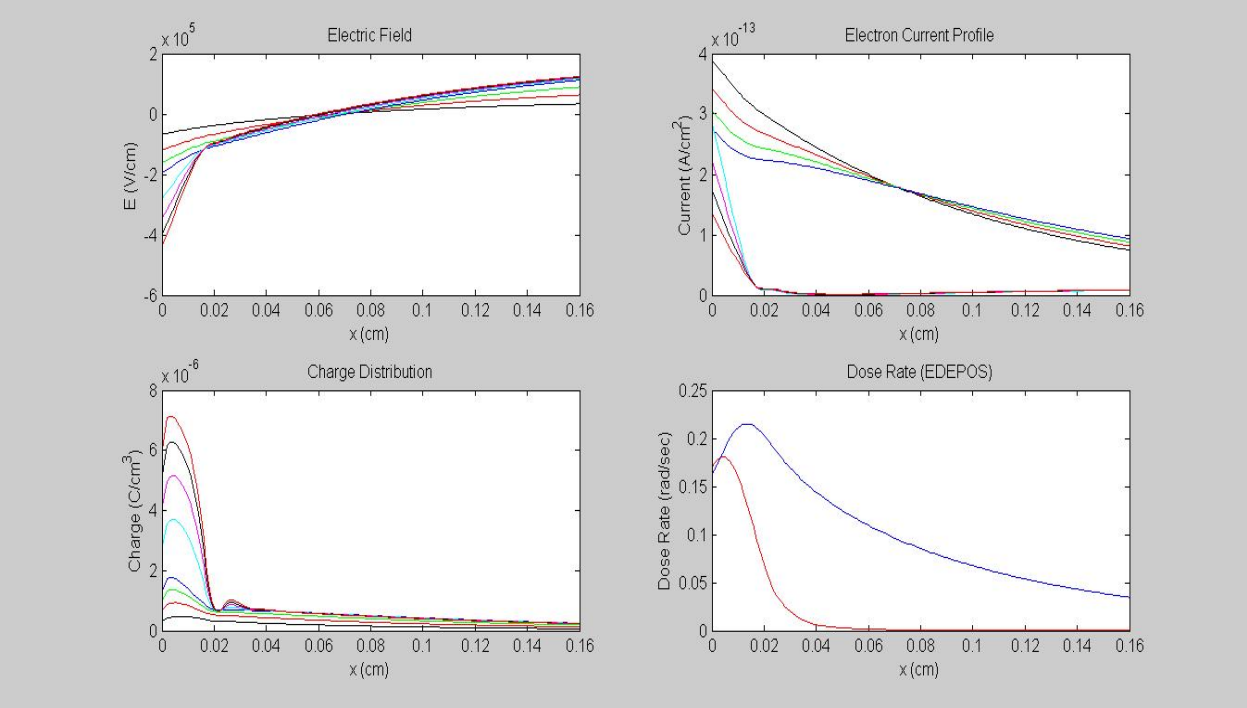

Figure 18. Simulation results with lower RIC after 4 days of "hard" and 4 days of "soft"

In a report of reasonable length, space does not permit the display of all the AF-NUMIT2 simulation runs that have been made with various paramters. Perhaps more helpful anyway is the summary chart in Figure 19 of the maximum electric field achieved during these runs. All runs were done using the CRRES spectra from Figure 16. The solid markers correspond to “hard-soft” or just “soft” spectra runs. The hollow markers were simulation runs made using a spectra for the entire run that was not designated as “hard” or “soft.” Most runs were for 8 days total, with a few for 10 days. The runs were long enough for equilibrium to be effectively achieved or until the electric field strength exceeded the assumed electrostatic threshold strength of 10^5 V/cm.

The results showed a dramatic and consistent dependence on the value of the RIC coefficient, increasing very proportionately to the reciprocal of the coefficient. As stated earlier, one should expect that less RIC would cause greater charging. Lower conductivity will result in less charge bleeding off the dielectric. The result is a higher electric field. Two runs (indicated with the solid blue square markers) were made with unrealistically high dark conductivity in order to verify this understanding. The higher dark current clearly caused charge bleed-off that negated the effect of the low RIC conductivity—these are the only points that do not fall on the straight trendline. Despite the expectation that higher fields will exist with lower conductivity, the consistency with which this relationship is observed, regardless of flux spectra, seems stunning to this author.

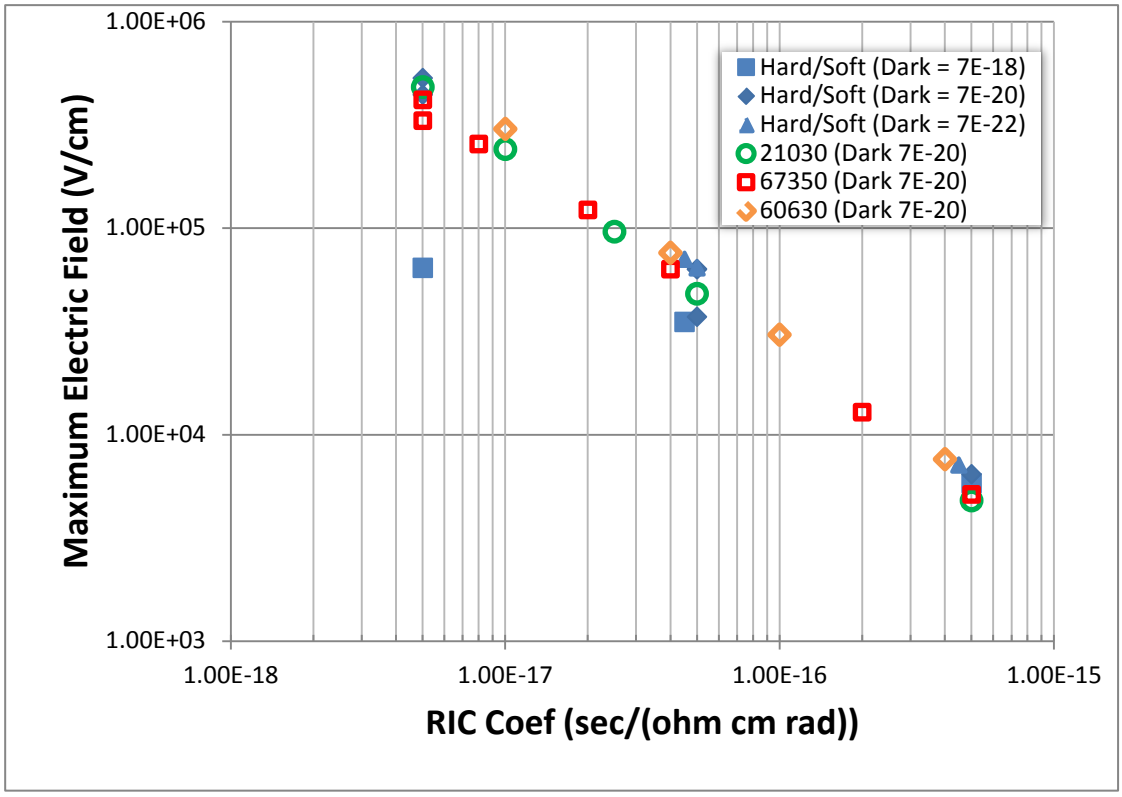

Figure 19. Summary of AF-NUMIT2 realistic simulation results

After these runs were performed, additional checks of the simulation time step size and spatial depth resolution were made. Using a smaller time step made no difference in the results whatsoever—strong indication that an appropriate choice had been made. However, particularly at lower incident energies, slightly different results were obtained when the model used a finer spatial depth resolution. Apparently, greater spatial resolution (moving from a spatial bin size from 10 μm to 1 μm) allowed the modeling of more charge closer to the surface. As a result, this charge was able to bleed off more rapidly causing a reduction in the maximum electric field by as much as 20 %. Unfortunately, increasing the resolution proportionately increases the actual run time so that the normal two minutes of run per simulated day becomes twenty minutes. More work needs to be done to find the optimal tradeoff between spatial resolution and practical run times—perhaps the time step size could be increased to compensate for greater resolution.

4.2 Other Issues Discussed with AFRL/RVBX but not in the SOW

4.2.1 Secondary Electron Yield. When high energy electrons strike the surface of a dielectric they can penetrate or backscatter, but they can also eject electrons that were part of the dielectric. The ejection of secondary electrons from near the surface of the dielectric certainly could cause a positive charging of the surface. Such an effect could be important in explaining or predicting the buildup of an electric field—particularly near the surface and particularly at very low incident electron energies (< 10 keV). Unfortunately, to the author's knowledge, not enough is known about secondary electron yield to be incorporated into a useful model. In addition, such a surface effect is not really part of a deep-dielectric charging model.

4.2.2 The Effect of Internal Electric Fields on Incident Electrons. Neither the original NUMIT nor AF-NUMIT2 incorporates in the model any retarding effect a growing electric field within the dielectric may have on later incident electrons. The depth profiles of charge and energy deposition ignore the existence of internal fields. Many discussions have occurred regarding the validity of this approximation.

In an earlier report,[14] this author presented an order-of-magnitude calculation that indicated any effect of an internal electric field in NUMIT would be less than 10 % until the threshold for electrostatic discharge is reached. However, in that same discussion it was pointed out that electrons at lower incident energies than NUMIT was modeling might be affected more greatly. Part of the present work is to extend NUMIT to lower energies, therefore this shortcoming of the NUMIT approach may now be more significant.

The significance of internal fields at lower incident energies, however, is not universally acknowledged. For example, Frederickson, Woolf, and Garth, wrote: "For electrons well below 100 keV, where the material stopping power dominates, the field effects are less important. It has been observed for electrons above 1 MeV that their trajectories are foreshortened in charged insulators." [21] Regardless of whether the issue of internal fields is more prominent at low or high incident electron energies, incorporating it into AF-NUMIT2 was not part of the proposed work.

4.2.3 A Better Model of Charge and Energy Deposition Profiles. As discussed in Subsection 3.7.4, it is clear that the best approach for determining the charge and energy deposition profiles is to do Monte Carlo simulations for isotropically incident electrons rather than piecing together simulations at individual angles of incidence. This approach would also incorporate backscatter

[14] Brian Beecken, "Development of the NUMIT Simulation for Modeling Deep-dielectric Charging in the Space Environment," presented to AFRL/RVBX, August 13, 2009.

off of the material's surface. It does require, however, a totally new algorithm that would fit to many, many MC simulations, thereby completely replacing EDEPOS and FredBell rather than just modifying them as done here.

David Barton of RVBX has begun a series of isotropic MC simulations at a wide range of energies for a wide range of materials. The hope is to eventually compile enough MC results that an entirely new algorithm can be devised and then implemented. Creating an algorithm that fits MC energy and charge deposition profiles for a variety of materials at a variety of energies would bypass the need to assume things like the isotropy of dielectrics and the need to sum multiple angular bins. In addition, since backscatter is included in the MC simulations, it would automatically be included in the algorithm that is fit to those simulations. Such an approach would create the basis of AF-NUMIT3 and be an exciting step forward in modeling of the deep-dielectric charging of spacecraft.

5.0 CONCLUSIONS

The work on development of AF-NUMIT2 has been performed and completed as proposed. The only exception is the inclusion in the model of time-dependent and temperature-dependent radiation induced conductivity. These dependencies were deemed by AFRL/RVBX as of lesser importance and their incorporation could be a negative feature due to the potential of misleading future users.

Going beyond the proposed work, AF-NUMIT2 has been tested extensively on Kapton over a wide range of possible conductivities, both dark and RIC, with the use of numerous electron energy flux spectra that are taken directly from the data compiled from CRRES measurements. An inverse proportional relationship between the RIC conductivity and the maximum internal electric field has been clearly, and rather unexpectedly, observed during the testing.

REFERENCES

[1] A. R. Frederickson, "Radiation-Induced Electrical Current and Voltage in Dielectric Structures," AFCRL-TR-74-0582, 1974.

[2] A. R. Frederickson, "Charge deposition, photoconduction, and replacement current in irradiated multilayer structures," *IEEE Trans. Nuc. Sci.*, vols. NS-22, p. 2556, 1975.

[3] T. Tabata and R. Ito, "An Algorithm for the Energy Deposition by Fast Electrons," *Nuclear Science and Engineering*, vol. 53, p. 226, 1974.

[4] A. R. Frederickson, J. T. Bell, and E. A. Beidl, "Analytic Approximation for Charge Current and Deposition by 0.1 to 100 MeV Electrons in Thick Slabs," *IEEE Trans. Nuc. Sci.*, vol. 42, p. 1910, 1995.

[5] J. F. Fowler, "X-ray induced conductivity in insulating materials," *Proc. R. Soc. London*, vol. A236, p. 464, 1956.

[6] A. R. Frederickson and C. E. Benson, "Improved testing procedures for spacecraft discharge pulses," in *Proceedings of the 7th Spacecraft Charging Technology Conference*, Noordwijk, The Netherlands, 2001.

[7] A. R. Frederickson, "New scaling laws for spacecraft discharge pulses," in *Proceedings of the 7th Spacecraft Charging Technology Conference*, Noordwijk, The Netherlands, 2001.

[8] E. J. Kobetich and R. Katz, "Electron Energy Dissipation," *Nucl. Instr. Methods*, vol. 71, p. 226, 1969.

[9] A. R. Frederickson, "Comparing CRRES internal discharge monitor results with ground tests and published guidelines," in *7th Spacecraft Charging Technology Conference*, Noordwijk, The Netherlands, April 2001.

[10] A. R. Frederickson, C. E. Benson, and J. F. Bockman, "Measurement of charge storage and leakage in polyimides," *Nuc. Inst. Meth. Phys. Res. B*, vol. 208, pp. 454-460, 2003.

[11] A. R. Frederickson and J. F. Bockman, "Conductivity measurements made on LARC-Si and Kapton polyimides for space applications," Report funded by NASA, RTOP 2.B.04.2, 3 September 2000.

[12] A. R. Frederickson and J. R. Dennison, "Measurement of Conductivity and Charge Storage in Insulators Related to Spacecraft Charging," *IEEE Trans. Nuc. Sci.* , vol. 50, no. 6, pp. 2284-2291, 2003.

[13] B. P. Beecken and J. McIver, "Extending the NUMIT Simulation for Modeling Deep-dielectric Charging in the Space Environment," in *Proc. of the 11th Spacecraft Charging Technology Conference*, Albuquerque, NM, September 2010 (Note: the author now believes subsections entitled "Determination of Electron Flux as a Function of Incident Angle" and "Application to NUMIT2" are incorrect.).

[14] I. Jun, H. B. Garrett, W. Kim, and J. Minow, "Review of an internal charging code, NUMIT," *IEEE Trans. Plasma Sci.*, vol. 36, no. 5, p. 2467, 2008.

[15] W. Kim, I. Jun, and H. Garrett, "NUMIT 2.0: the latest version of the JPL internal charging analysis code," in *Proc. of the 12th Spacecraft Charging Technology Conference*, Kitakyushu, 2012.

[16] B. P. Beecken and B. M. Wallin, "Modeling of Deep-dielectric Spacecraft Charging in Realistic Environments with NUMIT2," in *Proc of 3rd AIAA Atmospheric Space Environments Conference*, Honolulu, June, 2011 (Note: the author now believes subsection III.A.2 is incorrect.).

[17] V. A. Davis, M. J. Mandell, and R. H. Maurer, "Preliminary Surface and Internal Charging Analysis of the Radiation Belt Storm Probes Spacecraft," in *Spacecraft Charging Technology Conference*, Biarritz, France, 2007.

[18] W. Kim, I. Jun, and H. B. Garrett, "An Algorithm for Determining Energy Deposition Profiles in Elemental Slabs by Low (< 100 keV) Energy Electrons: An Internal Charging Application," *IEEE Trans. Nuc. Sci.*, vol. 55, no. 6, p. 3158, 2008.

[19] T. Tabata, R. Ito, and S. Okabe, "Generalized Semiempirical Equations for the Extrapolated Range of Electrons," *Nucl. Instr. Methods*, vol. 103, p. 85, 1972.

[20] D. C. Ferguson, T. A. Schneider, and T. A. Vaughn, "Effects of Cryogenic Temperatures on Spacecraft Internal Dielectric Discharges," in *Proceedings of the 1st International Conference on Space Technology*, Thessaloniki, Greece, August, 2009.

[21] A. R. Frederickson, S. Woolf, and J. C. Garth, "Model for Space Charge Evolution and Dose in Irradiated Insulators at High Electric Fields," *IEEE Trans. Nuc. Sci.*, vol. 40, no. 6, p. 1393, 1993.

APPENDIX A – User's Guide

This is a quick start-up guide to using AF-NUMIT2. All inputs that it refers to can be easily found in the first 100 lines of the code. For convenience, that code is reproduced in Appendix B.

Getting Started

AFNUMIT2.m is the main AF-NUMIT2 program. Open and run this in Matlab, but first verify the following.

4 Program Function Files that must be in the same folder as AFNUMIT2.m:

1. BeeckenTabFred.m Function predicts electron & energy deposition as a function of angle
2. getparameterB.m Function finds value of parameter B for electron deposition
3. backscatter.m Function that guesses at backscatter of incident electrons
4. num_der .m Function that takes a numerical derivative

Once the user verifies that the main program and its four function files are all in the same folder, then the AFNUMIT2.m file must be opened. The first choice that must be made is whether the user is starting a new run, or wants to add additional simulation time to a run that was just completed. The default is a new run, and so the first line of code is [`more = 'n'`]. Here the choice is set to "n" which stands for new or no. If the simulation run is to pick up where a previous run left off, the "n" is replaced with a "y" for yes.

Inputs Required From User

The parameters listed below must be typed into the code. If they are not typed into the code, the last used parameters will automatically be reused. The obvious advantage of this approach is that the user can easily make succeeding runs by simply using the file again, only changing what is needed. Plus, it will always be clear what parameters where chosen on the run just completed.

Required Characteristics of Dielectric Material
Thickness (cm)
Effective atomic number
Effective atomic weight
Density (g/cm^3)
Dark Conductivity [$1/(\Omega$ cm)]
Coefficient of RIC [sec/(Ω cm rad)]
Permittivity (F/m)

Resolution Control Settings

1. Isotropic vs. Beam: Either the incident electrons will be modeled as arriving isotropically, or they will arrive in a beam. If the choice is isotropic, then the number of angular bins must be set, thereby determining the angular resolution for isotropic incidence. Obviously choosing a greater number will also slow the simulation run time. It seems that 90 bins works well. If however, the choice is a beam to simulate a lab setting, then the number of angular bins must be set to 1. If it is a mono-energetic beam, then the flux units must be $1/(cm^2\ sec)$, but the option exists to have a multi-energetic beam in which case the flux units must be $1/(cm^2\ sec\ MeV)$. See electron energy flux spectrum below.
2. Time resolution is the time the charge deposited within the dielectric is allowed to move due to the electric fields before the electric fields are recalculated. It seems a time step of 0.1 seconds works well.
3. Spatial resolution (cm) is the distance between the nodes or bins that the material is divided into. Charge is considered to be stored in each bin. The value must be 0.001 cm or smaller, particularly for lower energies.

Electron Energy Flux Spectrum

A comma-delimited .csv file must be in the same folder as AFNUMIT2.m to specify the electron energy flux spectrum. The first cell of the file always is a zero. The rest of the first line contains the energy (MeV) of each channel of flux. The following lines give specific information about the time that a particular electron flux will be incident and the actual values of that flux. The first cell contains the time that that particular electron energy flux spectrum will run. The remaining cells contain the electron flux $1/(cm^2\ sr\ sec\ MeV)$ for each corresponding energy channel. (An example of this file structure is given in Table 1 in the main text.) After each row is simulated, a line will be plotted in all of the output graphs. If more plot lines are desired in order to observe the progression of the charging through time (for the same electron energy flux spectrum), simply divide the simulation time into the desired number of lines and repeat the row that many times.

For mono-energetic beams, the comma-delimited file only contains two columns. The top left is, as always, zero. The top right cell is the energy of the beam. The first cell in the second row is the time of simulation, as before, and the electron flux goes in the second column. Note that the electron flux now must have units of $1/(cm^2\ sec)$. For multi-energetic beams the same format is used as for isotropic, but the electron flux must have units of $1/(cm^2\ sec\ MeV)$.

After AFNUMT2.m is started, it will stop and ask the user to choose the electron energy flux spectrum .csv file from the directory.

Outputs

AFNUMIT2.m will output four plots in one .fig file:

1. Electric Field
2. Charge Distribution
3. Total Current
4. Dose Rate

A Matlab .fig file can be modified and reformatted extensively within Matlab, however, doing so requires some skill with Matlab. Therefore, AFNUMIT2.m automatically creates four .csv files corresponding to the four plots and saves them in the current folder. In addition to providing precise values for analysis, comma-delimited files can be imported into most any software and modified as desired. Before editing, it is strongly recommended that these files be moved to another folder due to the second purpose below.

The second purpose in creating the .csv results files is that they are used by AFNUMI2.m when it is decided to later continue the simulation run. To do so, the user must choose [`more = 'y'`] as discussed above. Note the files must be in the same folder as AFNUMIT2.m.

APPENDIX B – Actual Input Code

The first 100 lines of code are reproduced below so that the reader can easily identify the places to which the above instructions in Appendix A refer. These lines are mostly comments that primarily explain how to use AF-NUMIT2, concisely repeating the above instructions. All user inputs are included in these lines; the only reason to modify any other line of code in AFNUMIT2.m would be to actually change the program.

```
%%%%%%%%%%%%%%%%%%%%%%%%%%%%%%%%%%%%%%%%%%%%%%%%%%%%%%%%%%%%%%%%%%%%%%%%%%%%
%                                AF-NUMIT2
% The AF-NUMIT2 program calculates the one-dimensional motion of electrons
% within a dielectric material that is placed between two conducting
% surfaces. The NUMIT method divides the material into spatial nodes. For
% each spatial node:
%      1) The electric fields within the dielectric are calculated.
%      2) The resulting movement of charge between the nodes is calculated.
%      3) The new distribution of charge at each node is determined.
% The numerical calculations are iterated for each step in time. Hence the
% name NUMIT stands for "NUMerical ITeration." The approach was developed
% by A.R. Frederickson at the Air Force Cambridge Research Labs in 1974
% (AFCRL-TR-74-0582). For modeling of dielectric charging by electron
% bombardment, NUMIT requires the input from algorithms that predict the
% deposition profiles of the incident electrons and their energy.
%
% AF-NUMIT2 is a completely new version of Frederickson's NUMIT written by
% B.P. Beecken under the auspices of AFRL/RVBX and completed in 2013. It
% features re-derived transport equations and the ability to model an
% isotropic incident flux of electrons. The following functions are part of
% AF-NUMIT2:
%   BeeckenTabFred      - algorithm predicting electron and energy
%                            deposition as a function of angle
%   getparameterB       - algorithm interpolates a published table to find
%                         the value of parameter B for electron deposition
%   backscatter         - a guess at backscatter of incident electrons
%   num_der             - takes numerical derivative
%
%
%%%%%%%%%%%%%%%%%%%%%%%%%%%%%%%%%%%%%%%%%%%%%%%%%%%%%%%%%%%%%%%%%%%%%%%%%%%%

clear all;  % ensure no previously defined variables interfere
%close all; % close down all open graphing windows
%clc;       % clears main screen of any previous input

%%%%%%%%%%%%%%%%%%%%%%%%%%%%%%%%%%%%%%%%%%%%%%%%%%%%%%%%%%%%%%%%%%%%%%%%%%%%
%%%%%%%%%%%%%%%%%%%%%%%% INPUTS REQUIRED FROM USER %%%%%%%%%%%%%%%%%%%%%%%%%
%%%%%%%%%%%%%%%%%%%%%%%%%%%%%%%%%%%%%%%%%%%%%%%%%%%%%%%%%%%%%%%%%%%%%%%%%%%%
```

```
%%%%%%%%%%%%%% Return to previous simulation and continue? %%%%%%%%%%%%%%
% By default, every simulation is new so "more" = 'n', which stands for no
% or new.
% If the user wishes to continue a previous run, set "more" = 'y', for yes.
% During a continuation, the energy flux spectrum can change, but all
% material characteristics must be unchanged.
more = 'n';

%%%%%%%%%%%%%% Set material characteristics of dielectric %%%%%%%%%%%%%%

L = 0.16;           % total thickness of dielectric (cm)
Z = 6.3597;             % effective atomic number of dielectric
AW = 12.3922;         % effective atomic weight of dielectric
RHO_MAT = 1.42;      % dielectric density (g/cm^3)
V = 0;              % voltage difference between electrodes (V)
gDark = 7e-22;      % dark conductivity (1/ohm*cm)
gCoef = 4.5e-16;   % coef of radiation induced conductivity (sec/ohm*cm*rad)
epsilon = 3.4*8.854e-12; % permittivity (epsilon) of dielectric (F/m)

%%%%%%%%%%%%%% Set Model Parameters Controling Resolution %%%%%%%%%%%%%%

%%% Set Isotropic Incidence Resolution of Model %%%
% Set number of angular bins: use 1 for beams.
% For multi-energetic beams, the flux must be 1/(cm^2*sec*MeV).
% For mono-energetic beam, the flux must be 1/(cm^2*sec).
numberOfAngularBins = 1;

%%% Set Time Resolution of Model %%%
delta_t = 0.1;     % length of each time step (seconds)

%%% Set Spatial Resolution of Model %%%
delta_x = 0.001;    % distance between spatial nodes (cm)

%%%%%%%%%%%%%% Energy Spectrum & Incident Electron Fluxes %%%%%%%%%%%%%%
%%%%%%%%%%%%%%%%%%%%%% Input with a CSV "Data" file %%%%%%%%%%%%%%%%%%%%%%
logarithm = 'y';   % Energy channel width linear or logarithmic ('n' or 'y')
%
% INPUT CSV FILE LOCATION: must be in same folder as AF-NUMIT2
% INPUT CSV FILE DESCRIPTION: The cell that is the first col and row (i.e.,
% "top left") is ignored, but put a zero in it because comma-delimited
% files need a place holder. The first row of the matrix indicates the
% energy (MeV) of each channel. The second row and all following rows
% contain the electron flux in 1/(cm^2*sr*sec*MeV) at the particular energy
% designated in the first row, but the first cell is devoted to the time in
% seconds to be simulated at that energy spectrum.
% MULTI-ENERGETIC BEAMS: in this case the input CSV file is the same except
% that the electron flux in each energy channel must be in 1/(cm^2*sec*MeV).
% No Steradians! It is a beam.
% MONO-ENERGETIC BEAMS: in this case the input CSV file has only 2 columns!
% In the first row, as before, the first cell is zero and the second cell
% is the energy. After that, the first column is the time (sec) and the
```

```
% second column is the electron flux in 1/(cm^2*sec). No steradians. No
% energy beam width.
% FORMATTING OF PLOTS: after each row (which corresponds with an
% energy spectrum), NUMIT2 updates the plots. If more updates are desired
% (lines in the plots) for the same energy spectrum, simply create
% identical energy spectrum rows with appropriate times for plot intervals.
% OUTPUT CSV FILE LOCATION: placed in same folder as AF-NUMIT2

%%%%%%%%%%%%%%%%%%%%%%%%%%%%%%%%%%%%%%%%%%%%%%%%%%%%%%%%%%%%%%%%%%%%%%%%%%%%
%%%%%%%%%%%%%%%%%%%%%%%% USER INPUTS COMPLETED %%%%%%%%%%%%%%%%%%%%%%%%%%%%%
```

APPENDIX C – Important Variables in NUMIT2

	Variable Name	Variable Type	Meaning/Purpose	Source
User Inputs	L	number	Total thickness of dielectric (cm).	User specified.
	Z	number	Effective atomic number of dielectric.	User specified. See instructions for calculating.
	AW	number	Effective atomic weight of dielectric.	User specified. See instructions for calculating.
	gDark	number	Dark conductivity (g/ohm cm)	User specified.
	gCoef	number	Coefficient of radiation induced conductivity (sec/ohm cm rad)	User specified.
	RHO_MAT	number	Dielectric density (g/cm^3)	User specified.
	epsilon	number	Permittivity of dielectric (F/m)	User specified.
	numberOfAngularBins	Number	Resolution of isotropic model.	User specified. Setting to 1 models a beam. Caution: for beams make sure electron flux entered in Data array is in units of $1/(cm^2$ sec).
	delta_t	number	Length of each time step (sec).	User specified. Tradeoff accuracy vs. run time. If oscillation results, decrease.
	delta_x	number	Distance (cm) between the spatial nodes at which all values are calculated.	User specified. Tradeoff between spatial resolution and run time.
	Data	array	User specified energy spectra (MeV) and corresponding electron fluxes $1/(cm^2$ sr sec MeV). First cell blank. First row is the energy channels. Each subsequent row is another flux. The first column of each row is the number of seconds for that spectrum to be incident. [Note for beams electron flux must be in $1/(cm^2$ sec).]	User input CSV file.
Directly Determined by User Inputs	spectrumNumber	number	Increment used to keep track within largest loop the energy spectrum being used.	Increments between 1 and the *numberOfEnergySpectra* at beginning of main loop.
	numberOfEnergyBins	number	The number of energy channels in the spectrum (each with a specified flux).	Calculated from the number of columns in *Data*, less one.
	T0	row vector	Energy of electrons (MeV) for each channel in spectrum.	Each row of *Data*, after the first column.
	numberOfEnergySpectra	number	Number of potentially different energy spectrums and the number of lines on final plot.	Calculated from the number of rows in *Data,* less one.

	timeForEachEnergySpectrum	col vector	Time for flux from a particular energy spectrum to be incident on dielectric. It also is time between output plot lines.	First column of *Data*.
	J_incident	array	Incident electron flux [1/(cm^2 sr sec MeV)] for an energy channel. Each row could be a different flux, each column a different energy.	All but first column and first row of *Data*.
	J_incid	number	Incident electron current (A/cm^2) for a specific energy bin within a specific spectrum.	Calculated by taking a cell within the *Data* matrix and multiplying by appropriate conversion factors.
	x_value	col vector	Distance (cm) of each spatial node from surface.	Calculated by adding one *delta_x* for each spatial node.
	x_num	number	Number of spatial nodes	Size of vector *x_value*.
	EDEPOS	row vector	Energy deposited (MeV*cm^2/g) per electron in each spatial node.	Calculated by function TabFredBeecken for each energy and angle of incidence.
	Jofrac	row vector	Fraction of incident electrons passing through at each node	Calculated by function TabFredBeecken for each energy and angle of incidence.
	EDEPOS_angles	array	Energy deposited per electron on each node (row) for a specific angle (col).	Calculated from EDEPOS by taking the fraction of flux in that particular angular bin.
	Jofrac_angles	array	Fraction of incident flux on each node (row) for a specific angle (col).	Calculated from Jofrac by taking the fraction of flux in that particular angular bin.
	EDEPOS_iso	col vector	Total energy deposited per electron after summing all angles	Calculated by summing *EDEPOS_angles.* Could be replaced at this point by different algorithm source.
	Jofrac_iso	col vector	Total fraction of incident electrons after summing all angles	Calculated by summing *Jofrac_angles*. Could be replaced at this point by different algorithm source.
	rho_iso	col vector	Initial fraction of incident electrons deposited per unit time (C/(cm^3 sec))	Derivative of *Jofrac_iso*. Could be replaced at this point by different algorithm source.
	Dose_SumAngles	col vector	Dose (rad/sec) at each spatial node.	Calculated from *EDEPOS_iso* for each *J_incid*.
	Jo_SumAngles	col vector	Initial current (A/cm^2) at each spatial node.	Calculated from *Jofrac_iso* for each *J_incid*.
	rho_SumAngles	col vector	Initial charge deposited (C/cm^3) at each spatial node.	Calculated from *rho_iso* for each *J_incid* and multiplying by time increment. (Continuity Eq.)
	Dose_energies	array	Net initial dose rate for each energy channel (col) and at each spatial	Found by summing along the rows of *Dose_angles* for each

			node (row).	energy channel.
	Jo_energies	array	Net initial current (A/cm^2) for each energy channels (col) and at each spatial node (row).	Found by summing along the rows of *Jo_angles* for each energy channel.
	rho_energies	array	Net charge density (C/cm^3) for each energy channel (col) and at each spatial node (row).	Found by summing along the rows of *rho_angles* for each energy channel.
	Dose	col vector	Total dose rate for all angles and energies in one spectrum.	Sum across rows of *Dose_energies*.
	Jo	col vector	Total initial current for all angles and energies in one spectrum.	Sum across rows of *Jo_energies*.
	rho	array (2 cols)	Net charge density (C/cm^3) at each node, including previous charge depositions. Each row is node, and each column is a time step.	Sum across rows of *rho_energies* and add to previous depositions and/or results of charge transport (i.e., the time loop).
	E_Total	col vector	Total Electric field at each spatial node within dielectric.	Calculated in time loop from charge within dielectric and induced on electrodes.
	J	col vector	Total current at each spatial node within dielectric.	Calculated in time loop using Fowler model.
Outputs of Model	E_final	array	Electric field (V/cm) after each energy spectrum (col) to be plotted. Each row is a spatial node.	A col is appended for each *E_Total* calculated for each spectrum.
	J_final	array	Current (A/cm^2) after each energy spectrum (col) to be plotted. Each row is a spatial node.	A col is appended for each *J* calculated for each spectrum.
	rho_final	array	Cumulative charge density (C/cm^3) after each energy spectrum (col) to be plotted. Each row is a spatial node.	A col is added for each *rho* calculated for each spectrum.
	Dose_final	array	Net dose rate (rad/sec) after each energy spectrum (col) to be plotted. Each row is a spatial node.	A col is appended for each *Dose* calculated for each spectrum.

APPENDIX D – Calculating Effective Atomic Number and Weight for Compounds

Tabata defines the effective atomic number as

$$Z_{\text{eff}} = \sum_i f_i Z_i$$

and the effective atomic weight as

$$A_{\text{eff}} = \frac{Z_{\text{eff}}}{\sum_i f_i \frac{Z_i}{A_i}}.$$

Tabata says, "f_i is fraction by weight of the constituent elements." Following Tabata's reference to Rao, we find

$$f_i = \frac{n_i A'_i}{M}.$$

Here n_i is the number of atoms, A' is the atomic weight, and M is the molecular weight of the compound is given by

$$M = \sum_j n_j A'_j .$$

For example, the compound Kapton $C_{22}O_5N_2H_{10}$ has molecular weight M calculated by

$$M = 22(12.011) + 5(15.9994) + 2(14.0067) + 10(1.00794) = 382.332$$

The fraction by weight of the constituent elements are then:

$$f_C = \frac{22(12.011)}{382.332} = 0.6911 \qquad f_N = \frac{2(14.0067)}{382.332} = 0.0733$$

$$f_O = \frac{5(15.9994)}{382.332} = 0.2092 \qquad f_H = \frac{10(1.00794)}{382.332} = 0.0264$$

Finally then

$$Z_{\text{eff}} = f_C(6) + f_O(8) + f_N(7) + f_H(1) = 6.3597$$

and

$$A_{\text{eff}} = \frac{6.3597}{f_C(6/12) + f_O(8/12) + f_N(7/14) + f_H(1/1)} = 12.3922$$

DISTRIBUTION LIST

DTIC/OCP
8725 John J. Kingman Rd, Suite 0944
Ft Belvoir, VA 22060-6218 1 cy

AFRL/RVIL
Kirtland AFB, NM 87117-5776 2 cys

Official Record Copy
AFRL/RVBX/Dr. David Cooke 1 cy

This page is intentionally left blank.